Reprinted from

ORGANIC GEOCHEMISTRY

Vol. 7, *No.* 3/4, *pp.* 173–205

ORGANIC GEOCHEMISTRY OF DEEP SEA DRILLING PROJECT SEDIMENTS FROM THE GULF OF CALIFORNIA—HYDROTHERMAL EFFECTS ON UNCONSOLIDATED DIATOM OOZE

BERND R. T. SIMONEIT[1], R. P. PHILP[2], P. D. JENDEN[3] and E. M. GALIMOV[4]

[1]College of Oceanography, Oregon State University, Corvallis, OR 97331, U.S.A. [2]Institute of Earth Resources, CSIRO, Division of Fossil Fuels, North Ryde, N.S.W. 2113, Australia [3]Department of Earth and Space Sciences, University of California, Los Angeles, CA 90024, U.S.A. [4]V. I. Vernadsky Institute of Geochemistry and Analytical Chemistry, Academy of Sciences of the U.S.S.R., Moscow, U.S.S.R.

PERGAMON PRESS

OXFORD · NEW YORK · TORONTO · SYDNEY

PARIS · FRANKFURT

1984

rg. Geochem. Vol. 7, No. 3/4, pp. 173–205, 1984
inted in Great Britain.

0146-6380/84 $03.00+0.00
Pergamon Press Ltd

Organic geochemistry of Deep Sea Drilling Project sediments from the Gulf of California—Hydrothermal effects on unconsolidated diatom ooze

BERND R. T. SIMONEIT[1]*, R. P. PHILP[2], P. D. JENDEN[3]† and E. M. GALIMOV[4]

[1]College of Oceanography, Oregon State University, Corvallis, OR 97331, U.S.A.
[2]Institute of Earth Resources, CSIRO, Division of Fossil Fuels, North Ryde, N.S.W. 2113, Australia
[3]Department of Earth and Space Sciences, University of California, Los Angeles, CA 90024, U.S.A.
[4]V. I. Vernadsky Institute of Geochemistry and Analytical Chemistry, Academy of Sciences of the U.S.S.R., Moscow, U.S.S.R.

(*Received* 31 *August* 1983; *accepted* 18 *June* 1984)

Abstract—The effects of intrusive thermal stress have been studied on a number of Pleistocene sediment samples obtained from Leg 64 of the DSDP–IPOD program in the Gulf of California. Samples were selected from Sites 477, 478 and 481 where the organic matter was subjected to thermal stress from sill intrusions. For comparison purposes, samples from Sites 474 and 479 were selected as representative of unaltered material.

The GC and GC–MS data show that lipids of the thermally unaltered samples were derived from microbial and terrestrial higher-plant detritus. Samples from sill proximities were found to contain thermally-derived distillates and those adjacent to sills contained essentially no lipids. Curie point pyrolysis combined with GC and GC–MS was used to show that kerogens from the unaltered samples reflected their predominantly autochthonous microbial origin. Pyrograms of the altered kerogens were much less complex than the unaltered samples, reflecting the thermal effects. The kerogens adjacent to the sills produce little or no pyrolysis products since these intrusions into unconsolidated, wet sediments resulted in *in situ* pyrolysis of the organic matter.

Examination of the kerogens by ESR showed that spin density and line width pass through a maximum during the course of alteration but ESR *g*-values show no correlation with maturity. Stable carbon isotope ($\delta^{13}C$) values of kerogens decrease by 1–1.5‰ near the sills at Sites 477 and 481 and the atomic N/C decreases slightly with proximity to a smaller sill at Site 478. Differences in maturation behavior between Sites 477 and 481 and Site 478 are attributed to dissimilarities in thermal stress and to chemical and isotopic heterogeneity of Guaymas Basin protokerogen.

Key words: *n*-Alkanes, bitumen, Deep Sea Drilling Project, diatomaceous ooze, ESR, GC–MS, Guaymas Basin, hydrothermal alteration, lipids, molecular markers, protokerogen, pyrolysis, stable carbon isotopes, thermal stress.

INTRODUCTION

Leg 64 of the Deep Sea Drilling Project—International Phase of Ocean Drilling (DSDP–IPOD) program was designed to investigate three major geological environments in the Gulf of California (Curray *et al.*, 1982). These can be summarized:

(1) *Baja California* (Cabo San Lucas): Typical passive margin, with some intrusive sills (Sites 474, 475 and 476).
(2) *Guaymas Basin:* Spreading center with high heat flow, sills and turbidites (Sites 477, 478 and 481).
(3) *Guaymas Continental Slope:* Oxygen-minimum zone on continental slope (Sites 479 and 480). At Site 480 the hydraulic piston corer provided undisturbed laminated sediments (Schrader *et al.*, 1980).

The drilling locations of the sites in this study are shown in Fig. 1. A brief description of the geology and lithology is given below and summarized in Figs 2–5.

Baja California–Cabo San Lucas Sites

Sites 474–476 were drilled along a transect of the Baja California continental margin. Site 474 is located on oceanic crust, overlain by 500 m of diatomaceous mud and turbidites at a water depth of 3023 m. Sites 475 and 476 were drilled on the lower continental slope at 2631 and 2400 m water depths, respectively. Both sites penetrated primarily hemipelagic sediments and a minor carbonaceous mudstone overlying a conglomerate. The geological structure of this margin is dominated by horst-and-graben tectonics and by listric faulting. Sites 475 and 476 lie on the two lowest and most deeply-subsided blocks (Curray *et al.*, 1982).

Guaymas Basin

The Guaymas Basin is an actively spreading ocean basin that includes two well-defined rifts separated by a 20-km-long transform fault (Curray *et al.*, 1979, 1982). High sedimentation rates keep the basin floor covered while new ocean crust forms. Sites 477 and 481 are located in the southern and northern rifts, respectively, while Site 478 is adjacent to the transform fault zone on slightly older crust just north of the southern rift (Curray *et al.*, 1979, 1982). The

* Author to whom correspondence should be addressed.
† Present address: Global Geochemistry Corporation, 6919 Eton Avenue, Canoga Park, CA 91303, U.S.A.

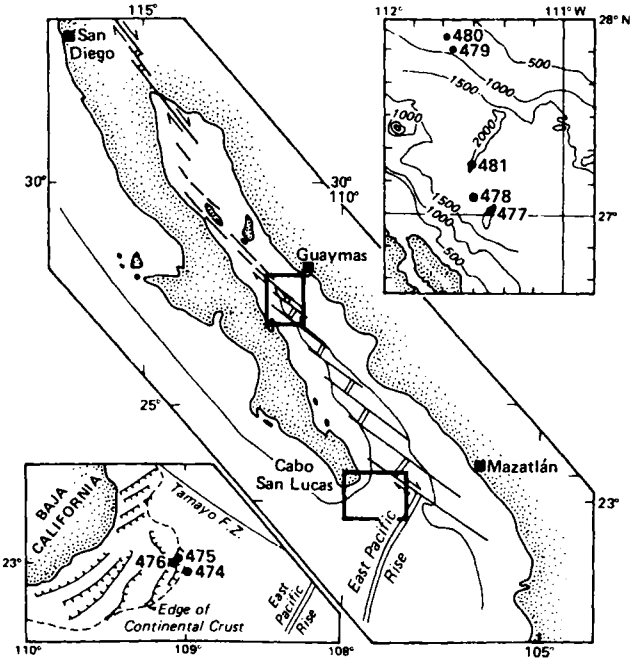

Fig. 1. Location map for the Leg 64 drill sites at the mouth and in the central Gulf of California.

sediments are diatomaceous oozes and turbidites, intruded by dolerite sills. Site 477 had the highest heat flow (20 HFU), and Site 481 had slightly higher heat flow than Site 478 (about 4 HFU).

Guaymas Slope

Sites 479 and 480 are on the Mexican continental slope north of Guaymas Basin within the present oxygen-minimum zone. Laminated diatomaceous sediments are deposited throughout the northern Gulf of California, wherever the oxygen-minimum zone contains less than 0.2 ml/l O_2 (Calvert, 1964). Alternations of laminae rich in diatoms or in terrigenous clay apparently reflect seasonal variations in productivity and/or runoff (Calvert *et al.*, 1964, 1966). Lamination is a response to both source variations (marine versus terrigenous input) and preservation (a reducing or anoxic water column prevents significant bioturbation and favors preservation of organic matter). Sites 479 and 480 provided detailed sampling of these laminated sequences. They contain information on past climatic changes and cycles, circulation patterns, depth or intensity of development of the oxygen-minimum zone, sea level, diagenesis, and the floral and faunal assemblage of surface and bottom waters. Alternations of laminated and non-laminated zones are probably responses to changes in the degree of oxygenation of bottom waters. The deeper sections at Site 479 are more indurated than the shallow sections and thus have been less disturbed by drilling. Laminated sediments continue to the bottom of the hole.

APPROACH

This paper presents an overview of the organic geochemistry of these sites. Particular attention is devoted to the evaluation of two major topics: (1) the sources and characteristics of the organic matter; (2) the effects of thermal stress on that organic matter. The sources and characteristics of the organic matter can be determined by analyzing the lipid fractions for homologous compound distributions, types of molecular markers and the nature of the unresolved mixtures (Simoneit, 1975, 1978, 1982a,b), and by analyzing the kerogens for their bulk compositional properties (e.g. elemental analysis, ESR, etc.), as well as by pyrolysis–gas chromatography (GC), and pyrolysis–GC–mass spectrometry (MS) (e.g. van de Meent *et al.*, 1980). The effects of thermal stress on the organic matter can also be evaluated by these same lipid and kerogen analyses. These data can then be correlated with the interstitial hydrocarbon gas (C_1–C_7) composition. The effects of the intrusive sills on the organic matter have been examined by Curie-point pyrolysis (Cupy), electron spin resonance spectroscopy (ESR), stable carbon isotope composition and elemental analysis.

Recently, pyrolysis has become a powerful analytical tool, especially in studying macromolecular materials (Irwin, 1979a,b). Increased applications of pyrolysis are the result of fast microscale flash pyrolysis techniques that appear to yield predominantly degradation products (Jones and Cramers, 1977). Pyrograms, obtained either by Cupy–GC or

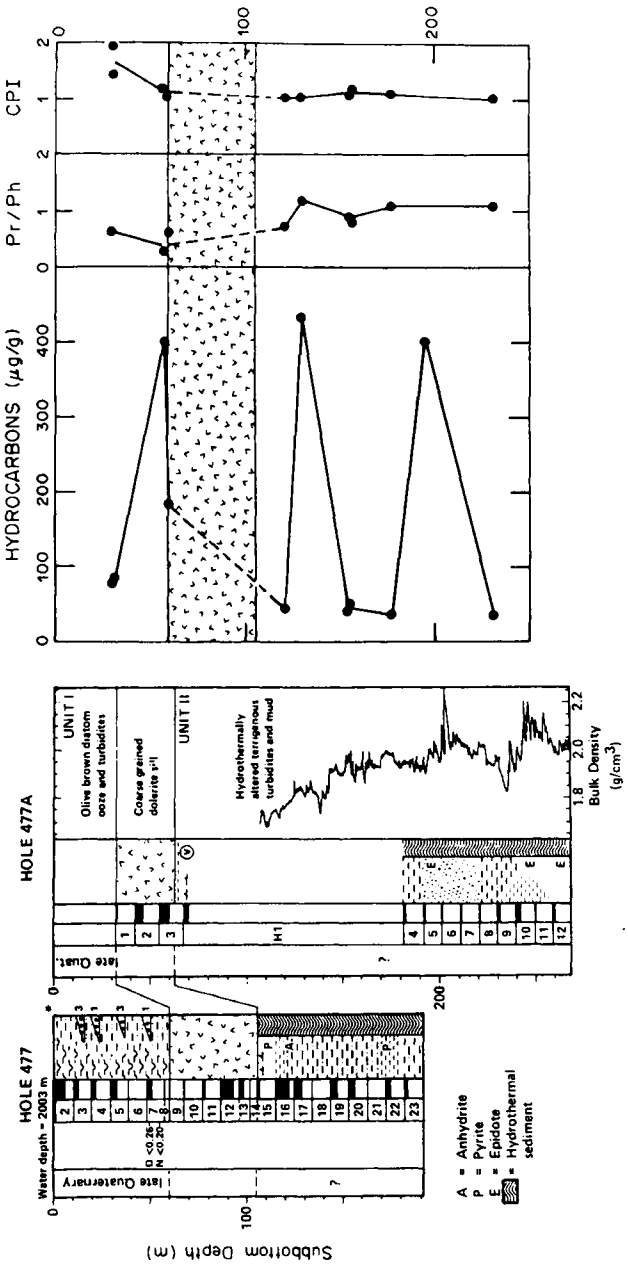

Fig. 2. Lithologic column, bulk density log, and trends of hydrocarbon concentration, pristane-to-phytane ratio, and carbon preference index (CPI) versus depth for Site 477.

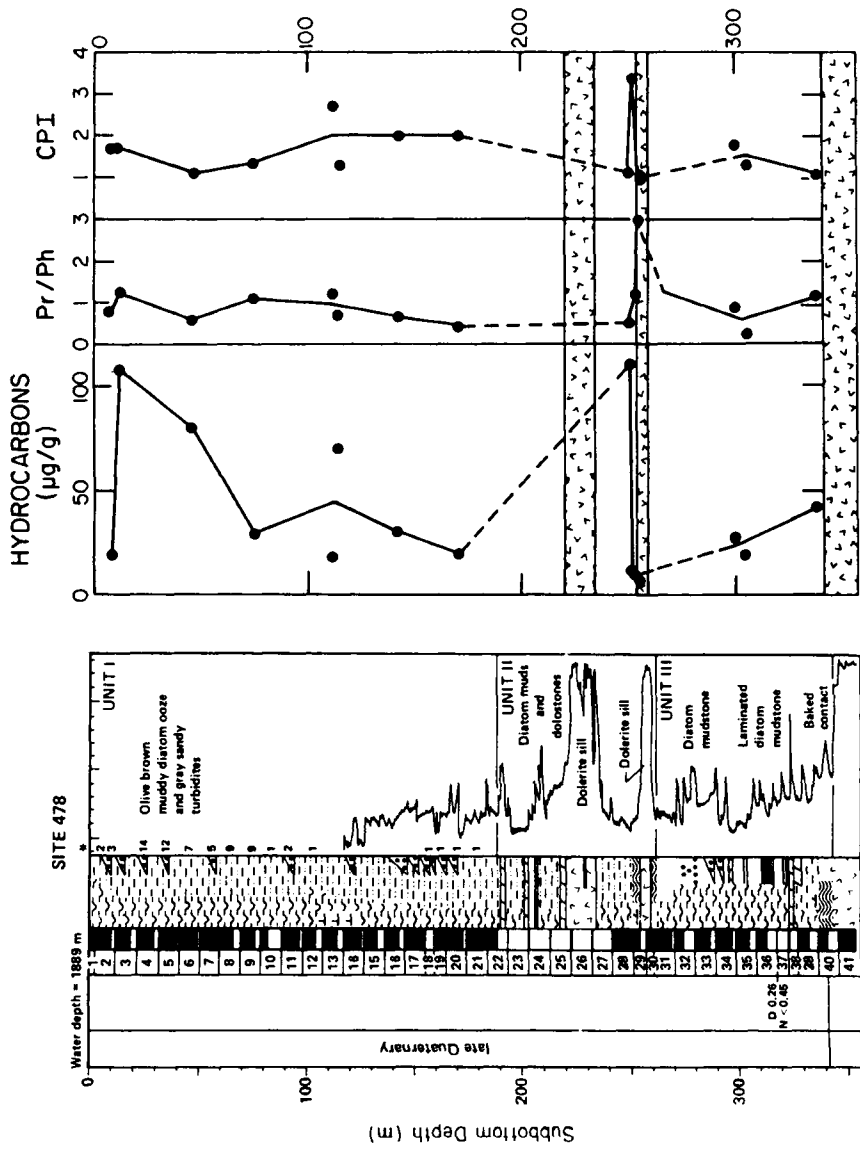

Fig. 3. Lithologic column, bulk density log, and trends of hydrocarbon concentration, Pr/Ph, and CPI versus depth for Site 478.

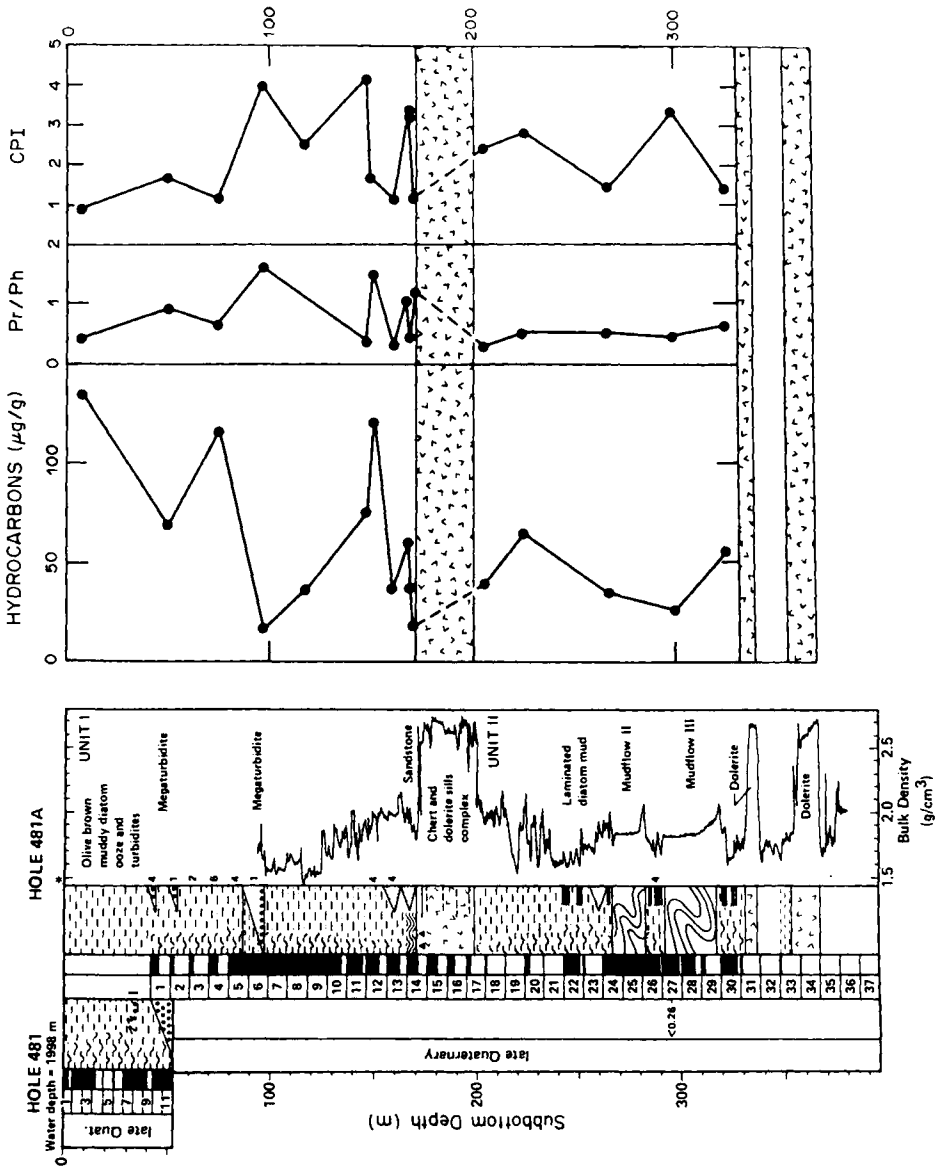

Fig. 4. Lithologic column, bulk density log, and trends of hydrocarbon concentration, Pr/Ph, and CPI versus depth for Site 481.

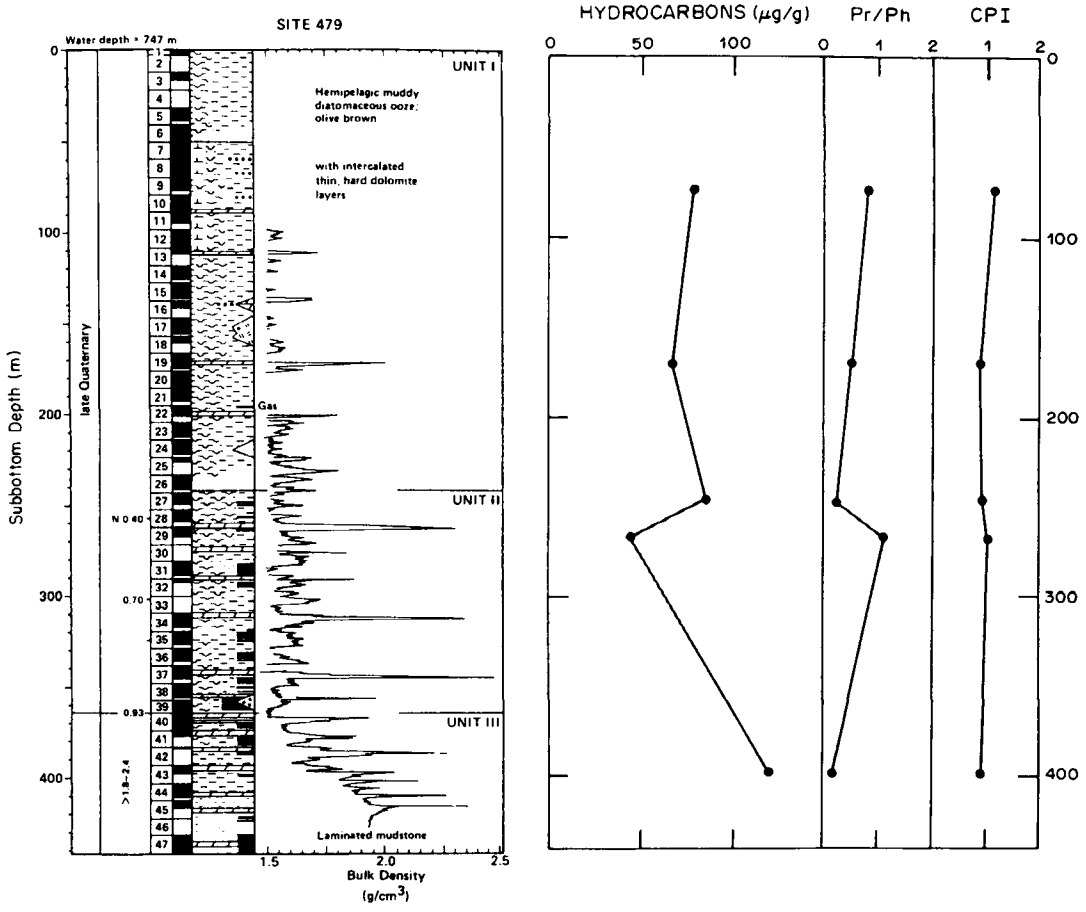

Fig. 5. Lithologic column, bulk density log, and trends of hydrocarbon concentration, Pr/Ph, and CPI versus depth for Site 479.

Cupy–MS, are sufficiently reproducible and specific to characterize synthetic polymers, biopolymers, and geopolymers. To relate thermal degradation products to the original macromolecule, it is necessary to identify the products and understand how they are formed. Cupy–GC–MS (Simmonds *et al.*, 1969) and pyrolysis high-resolution MS, using field ionization and field desorption (Schulten *et al.*, 1973, 1978), have yielded much structural information on thermal degradation products of various types of macromolecular materials. The general reaction mechanisms that form pyrolysis products are only poorly understood, although recently substantial advances have been made (Posthumus *et al.*, 1974; Posthumus and Nibbering, 1977; DeJongh, 1977). Despite this shortcoming, pyrolysis techniques have been successfully used to study biopolymers (Meuzelaar *et al.*, 1977), humic substances (Bracewell *et al.*, 1976), and kerogens (Maters *et al.*, 1977; Larter and Douglas, 1978). More recently, Cupy, with GC and GC–MS, has been utilized to characterize protokerogens from Recent algal mats and kerogens from DSDP core samples and ancient sediments (van de Meent *et al.*, 1980).

Various other micro-scale pyrolysis–GC techniques have been used recently to characterize petroleum source rocks and kerogens (Whelan *et al.*, 1980; Huc *et al.*, 1981) and to study the effects of clays on hydrocarbon generation (Davis and Stanley, 1982). Larter (1984) has reviewed the application of pyrolysis to kerogen characterization and fossil fuel exploration.

METHODS

Lipids

Small samples of cores were dried onboard ship in an oven at 45°C for C, H, N analysis and were then extracted with methylene chloride (CH_2Cl_2) for this study. Larger samples were freeze-dried and repeatedly extracted with a chloroform and methanol mixture (1 : 1) by ultrasonication. The extracts were concentrated on a rotary evaporator and treated with BF_3 in methanol to derivatize free fatty acids. The extracts were then subjected to thin-layer chromatography (TLC) on silica gel; hexane and diethyl ether mixture (9 : 1) was used as the eluent. After development with iodine vapor the bands corres-

ponding to hydrocarbons, esters and ketones were scraped from the TLC plates and extracted with methylene chloride. The hydrocarbon and combined ester and ketone fractions were analyzed by GC and GC–MS.

GC analyses were carried out on a Hewlett-Packard 5830 gas chromatograph using a 25 m × 0.20 mm fused silica capillary column coated with SP-2100 and programmed from 35 to 280°C at 4°C/min; He was the carrier gas. GC–MS analyses were performed on a Finnigan 4000 quadrupole mass spectrometer interfaced directly to a Finnigan 9610 gas chromatograph equipped with a 30 m × 0.25 mm fused silica capillary column coated with SE-54. The GC conditions for the GC–MS analyses were the same as those employed in the analytical GC system and the mass spectrometer was scanned at 0.95 sec/decade. The mass spectrometric data were acquired and processed with a Finnigan–Incos 2300 data system.

Kerogen

The exhaustively-extracted samples were treated with 3 M HCl and warmed to approximately 60°C for 1 hr. The acid was removed, and the residue was washed with distilled water and dried. After weighing, the sample was treated with aliquots of 3 M HCl and 50% HF in a 1 : 1 ratio until no further weight loss of the residue was recorded. Finally, the kerogen concentrate was re-extracted with CH_2Cl_2 to remove any entrapped lipids. The extracts obtained after the acid treatment were evaporated to dryness (cf. Simoneit and Philp, 1982, for yields of each fraction) and were not analyzed further. No attempt was made to isolate humic and fulvic acids from these small kerogen fractions. It is assumed that the humic and fulvic acids become incorporated into the kerogen under increased thermal stress, thus all macro-molecular organic matter is termed kerogen in this paper.

Cupy–GC with Cupy–GC–MS

The exhaustively extracted kerogens were subjected to pyrolysis–GC analyses using a Pye Curie-point pyrolyzer coupled to a Hewlett-Packard 5710 GC. Nickel/iron alloy wires were used in the pyrolyzer to produce a pyrolysis temperature of 610°C for 12.5 sec (van de Meent *et al.*, 1980). The GC was equipped with a fused silica capillary column (50 m × 0.3 mm o.d.) coated with SE-30. Temperature conditions were as follows: Ambient for 2 min; 70°C for 2 min; programmed at 4°C/min to 260°C.

Cupy–GC–MS of selected kerogens was performed using a Pye Curie-point pyrolyzer coupled to a Finnigan 4023 GC–MS system equipped with a Finnigan–Incos 2300 data system. Kerogens were selected on the basis of Cupy–GC results. Those producing only small concentrations of pyrolysate were not analyzed further by Cupy–GC–MS. Alloy wires of Ni/Fe were used with the pyrolyzer to give a pyrolysis temperature of 610°C for 12.5 sec. A 30-m SP-2100 WCOT capillary column was used in the GC–MS system, and the temperature was programmed from 100 to 270°C at 4°C/min. The separator (interface line) temperature was 250°C, the ion source temperature was 260°C, the filament current was 250 μA, the electron energy was 70 eV, and the scan speed was 0.95 sec/decade.

ESR Analyses

For electron spin resonance (ESR) analyses, kerogens were sealed under vacuum in 4 × 3 mm quartz tubes and scanned using a Varian E-12 spectrometer. The spectra were recorded at a microwave frequency of 9.5 GHz and a power output of 2 mW. The magnetic field was modulated at 100 kHz frequency and 5 gauss amplitude, and absorption occurred around 3380 gauss. The line width, ΔH, was measured between extremes of the first derivative absorption spectrum. Varian strong pitch standard (0.1% in KCl) was used to calibrate g-value and spin concentration measurements. To calculate g-value the following formula was used:

$$g_{\text{sample}} = g_{\text{standard}} \left[\frac{H_{\text{standard}}}{H_{\text{sample}}} \right]$$

where H refers to the magnetic field strength at maximum resonance.

Spin concentration, N, was assumed to be proportional to the first derivative absorption intensity, I, times the line width, ΔH, squared (Chesnut, 1977):

$$N \propto I\,(\Delta H)^2$$

Values were normalized to percent carbon in the kerogens.

Stable Carbon Isotope Analyses

For carbon isotope analysis, 10 mg samples of kerogen were combusted at 850°C in 7 × 9 mm quartz tubes in the presence of CuO wire and Ag foil (Frazer, 1962). Carbon dioxide was purified, measured, and collected on a vacuum line for analysis using a Varian MAT 250 stable isotope ratio mass spectrometer.

Elemental Analyses

The kerogens were found to average only 10–15% carbon, so that further purification was required to prevent erroneous H/C determinations (Durand, 1980a; Durand and Monin, 1980). Digestion for 24 hr in an aqueous solution of 25% $AlCl_3 \cdot 6H_2O$ dissolved large amounts of fluoride minerals precipitated during HF treatment (Jenden, 1983). After water washing and lyophilization, macroscopic pyrite was removed from samples taken from Cores 477-22, 477A-5, 477A-9, 478-13 and 478-40, and from Sections 478-29-1 and 478-29-2 (slick) by density separation in bromotrichloromethane, $CBrCl_3$ (specific gravity ~2). The heavy liquid was removed by cutting

and rinsing with hexane and the kerogen was dried under a stream of nitrogen gas. These procedures raised the average carbon content in the kerogen to approximately 40%. Samples from Site 477 and Section 481-11-2 were sent to the Microanalytical Laboratories at the University of California, Berkeley, for carbon, hydrogen and nitrogen determination. The remaining samples were analyzed at UCLA according to the methods outlined in Frazer (1962) and Peters (1978).

RESULTS AND DISCUSSION

The samples in this study are listed in Tables 1 and 2 with a summary of various parameters obtained for each sample. In the first part of this discussion the results of the lipid analyses from the surface samples are detailed prior to examining the effects of the intrustions on the lipids at greater depths in the drill sites. The second part focuses on the bulk chemistry of the kerogen fractions and examines the effects of intrusive thermal stress on these kerogens.

Lipids in Surface Samples from Sites 474, 477 to 479, and 481

Examples of *n*-alkane distributions from these sites are shown in Figs 6–8, and the hydrocarbon yields, CPI and Pr/Ph data are plotted in Figs 2–5 (CPI = carbon preference index; Cooper and Bray (1963); Pr/Ph = pristane-to-phytane ratio; Didyk *et al.* (1978)).

The lipids of the surface samples from the mouth of the Gulf of California are primarily of a marine autochthonous origin (Simoneit, 1982c; Galimov *et al.*, 1982). This is based on the *n*-alkanes which are derived mainly from microbial sources, with only a minor higher-plant wax component.

The shallow samples from Sites 477 and 478 contain roughly equal proportions of lipids from marine and terrestrial sources. In general, the *n*-alkanes (e.g. Figs 6 and 7) range from C_{12} to C_{35}, with maxima at C_{19}, C_{22} and C_{29}, and a strong odd-to-even carbon-number predominance $>C_{24}$. The lower molecular weight homologs ($<C_{25}$) and the associated unresolved complex mixture (hump), represent primary and degraded detritus from microbiota; the higher homologs are from vascular plant waxes (Simoneit, 1975, 1978, 1981; Galimov *et al.*, 1982). The predominance of *n*-nonadecane (*n*-C_{19}; Figs 6 and 7) may indicate an unaltered, primary bacterial residue. Phytane is the predominant isoprenoid hydrocarbon (Pr/Ph < 1; Figs 2 and 3) and varying amounts of sulfur and perylene are also present, indicating partially euxinic paleoenvironmental conditions of sedimentation (Didyk *et al.*, 1978). Perylene is common in Recent sediments. It probably indicates deposition under anoxic conditions, where it may derive from possible biogenic precursors of either a marine or terrigenous origin (Simoneit *et al.*, 1982; Baker and Louda, 1982). The presence of organic and/or elemental sulfur is, however, less definitive for paleoenvironmental conditions but does indicate a low level of oxygen (i.e. euxinic). This agrees with the lithological interpretation of an organic-rich sediment influx into the Guaymas Basin (Curray *et al.*, 1979, 1982), leading to euxinic conditions where not all the organic matter can be fully degraded. The high phytane content of sample 477-7-1, 124–126 cm is typical of sapropelic sediments deposited under strongly euxinic conditions (e.g. Simoneit, 1977a, 1981; Simoneit *et al.*, 1979).

The samples from Sites 479 and 480 contain lipids which are immature, but appear to mature versus depth (Galimov *et al.*, 1982; Simoneit, 1983). Approximately equal proportions of autochthonous marine and allochthonous terrigenous *n*-alkanes are present. For Site 479 and Pr/Ph is less than one, and both perylene and sulfur are present, again indicating partially euxinic paleoenvironmental conditions (Simoneit, 1983). The overall hydrocarbon yield increases slightly versus depth, while both the Pr/Ph and CPI appear to decrease (Fig. 5).

At Site 481, the lipids are derived from terrestrial sources. The *n*-alkanes (Fig. 8) range from C_{11} to C_{35}, with maxima at C_{17} and C_{29} and have a strong odd-to-even carbon number predominance $>C_{23}$. The minor components $<C_{21}$ are from degraded microbial detritus, and the significant odd-carbon *n*-alkanes ($>C_{23}$) are derived from vascular plant waxes (Simoneit, 1975, 1978, 1981). The distributions are similar to some of the surface samples from Site 30G (about 8 km to the northeast, Simoneit *et al.*, 1979), and the terrestrial-wax component may originate primarily from grassland and forest vegetation. The Pr/Ph is about one (Fig. 5) and some sulfur, but no perylene, occurs. This indicates partially euxinic conditions resulting from the high and varying influx of sedimentary detritus by turbidite transport, which leads to limited degradation and thus, greater preservation of organic matter.

Molecular markers

The influx of a minor terrestrial component from resinous plants to the Guaymas Basin and Slope is confirmed by the presence of dehydroabietic acid (Stucture **I**, Appendix) (Simoneit, 1983; Simoneit and Philp, 1982). It is the dominant molecular marker of resinous higher plants (Simoneit, 1977b), and occurs in all the shallow samples and at Site 30G (Simoneit *et al.*, 1979). Dehydroabietic acid was not detected in the samples from the mouth of the Gulf of California (Simoneit, 1982c).

Examples of *m/z* 191 mass chromatograms are shown in Fig. 9 to illustrate the major changes. The triterpenoids in the shallow samples at Site 477 are primarily the thermally mature 17α(H)-hopanes (**II**) with lesser amounts of 17β(H)-hopanes (**II**) and various hopenes and moretanes (e.g. Fig. 9d). In comparison, the triterpenoids of shallow samples

from Sites 478, 479 and 481 are dominated by the 17β(H)-hopanes (**II**) and the *neo*-hopanes (**III**) (also *iso*-hopanes), with significant amounts of various triterpenes (e.g. **IV**), moretanes (**V**) and 17α(H)-hopanes (e.g. Figs 9a and 9b). These triterpenoid distributions correlate with those at Site 30G (Simoneit *et al.*, 1979) and they reflect an origin primarily from autochthonous microbiota (Simoneit, 1978, 1984). The preponderance of the 17β(H) stereochemistry for the hopanes and the presence of olefins confirms the immaturity and in this case the Recent origin of these molecular markers. *Iso*-hop-13(18)-ene (**VI**) appears to be an unaltered marker compound derived from microbiota (Howard, 1980; Howard *et al.*, 1984) rather than from allochthonous sources (e.g. ferns; Ageta *et al.*, 1968).

Minor amounts of sesquiterpenoid (e.g. cadalene, **VII**) and diterpenoid hydrocarbons (e.g. dehydroabietane, **VIII**; dehydroabietin, **IX**; retene, **X**; simonellite, **XI**) occur in all samples. Their concentrations are highest in the shallow and immature samples. These molecular markers are derived primarily from terrestrial resinous plants (Simoneit, 1977b). Extended tricyclic terpanes (**XII**) are detectable in only a few thermally altered samples (from Sections 477A-5-1, 477A-9-1, and 481A-14-3), and they appear to be derived from unknown biogenic precursors, occurring with the 17α(H)-hopane series.

Steroidal derivatives are found mainly in the hydrocarbon fractions. Typical examples of various mass chromatograms are shown in Fig. 10. The steranes in the shallow samples at Site 477 indicate significant maturation, probably caused by the very high thermal gradient at this site (e.g. Fig. 10b; Mackenzie *et al.*, 1982a). The major steranes are the 5α and 5β,14α,17α(H) homologs (**XIII**, R = H, 20R stereochemistry) ranging from C_{26} to C_{30} with a predominance of cholestane. These steranes are of a marine source, based on their ternary distribution (Huang and Meinschein, 1979). No sterenes are present, although small amounts of 4-methylsitostane (**XIII**, R = CH_3, R′ = C_2H_5) and diasterenes (**XIV**, e.g. Fig. 10e) ranging from C_{27} to C_{29} are found. The advanced maturity of the bitumen from samples near the sill at Site 477 is also confirmed by other steroid derivatives. For example, the ring C monoaromatic steranes (*m/z* 253, Fig. 10c) are present at significant concentrations, as are the triaromatic steranes (suggested structure **XV**, *m/z* 231, Fig. 10d). The aromatization ratios, as proposed by Mackenzie *et al.* (1982b) for the 5α(H) and 5β(H) isomers of (24R/S)-(20R)-24-ethyl-17β-methyl-18-norcholesta-8,11,13-triene to the (24R/S)-(20R)-24-ethyl-17β-methyl-18,19-dinorcholesta-1,3,5(10),6,8,11,13-heptaene, range from 15 to 20% for these samples. The C-20 isomerization ratios of (24R/S)-(20R)-24-ethyl-5α(H),14α(H),17α(H)-cholestane (Mackenzie *et al.*, 1982b; Seifert and Moldowan, 1979) vary from 5 to 10% for these samples.

The immaturity of the surface sediments at Sites 478, 479 and 481 is indicated by the predominance of sterenes (e.g. Fig. 10a), some steradienes and 5α(H),14α(H),17α(H)-steranes (**XIII**, R = H, 20R). The sterenes are comprised of primarily the Δ^4 and Δ^5 isomers (**XVI**) ranging from C_{27} to C_{29} and the steradienes consist of the $\Delta^{5,22}$ isomers, also with the same range and relative distributions. The more pronounced influx of terrigenous detritus to these sites is indicated by relatively higher concentrations of the C_{29} steroids (Huang and Meinschein, 1979).

Tetrapyrole pigments are the most sensitive indicators for the thermal history of sedimentary organic matter (Baker and Louda, 1982, 1983) and the trend is illustrated for Site 477 in Fig. 11 with typical UV-visible spectra. The pigments in the shallow and immature samples consist of chlorins (Galimov *et al.*, 1982; Galimov and Kodina, 1983).

Stable carbon isotope data

The carbon isotope distribution between various bitumen fractions is characterized by a regular depletion of ^{12}C with increasing polarity of the bitumen fraction (Galimov *et al.*, 1982; Galimov and Kodina, 1983). Some examples of this depletion trend are shown in Fig. 12 and, as thermal stress increases, the trend inverts. The overall $\delta^{13}C$ data for the immature lipid fractions from all sites are in the range of −23 to −24‰, typical of primarily marine organic matter (Galimov, 1974; Galimov *et al.*, 1982).

HYDROTHERMAL EFFECTS OF INTRUSIONS ON LIPIDS

Site 477

The hydrocarbon yields, CPI, Pr/Ph ratios and *n*-alkane distributions for selected samples from Site 477 are shown in Figs 2 and 6, respectively. The differences in hydrocarbon distributions (Fig. 2) approaching the sill are quite dramatic. Near the sill a thermogenic component appears, which shows no carbon number predominance and ranges from C_{20} to C_{33}, with a maximum at C_{25} (Fig. 6). Compared to immature samples, the wax alkanes with an odd carbon number predominance have disappeared. Phytane is predominant, and the C_{17} and C_{19} hydrocarbons indicate a microbial remnant. A broad, unresolved mixture (hump) of hydrocarbons characterizes the GC traces of these and the following samples—further evidence of a thermogenic component. Similar hydrocarbon distributions occur below the sill in the high-heat-flow zones of Holes 477 and 477A. With increasing subbottom depth and temperature, these hydrocarbon distributions reflect primarily the effects of extensive (>350–400°C) hydrothermal activity. Maxima in hydrocarbon concentrations are evident above and below the sill and at greater depth, although the sample density is limited (cf. Fig. 2). These hydrocarbon distributions differ from those of an intruded, semilithified, Cretaceous

Table 1. Sample descriptions and results of whole sediment analyses, Central Gulf of California, Leg 64

Sample designation	Sub-bottom depth (m)[a]	Lithology and age	Carbon (%)[b] Total	Organic	$CaCO_3$ (%)[b]	N/C (C/N)	Lipids free (μg/g)[c]	*n*-Alkanes Total (μg/g)	CPI[d]	Max[e]	Pr/Ph[f]	*n*-Fatty acids Total (μg/g)	CPI[d]	Max[e]
477-5-1 (81–91,94–96 cm)	30.4 (36.7)	Diatom. ooze Late Pleist.	3.6	2.6	8	0.077(13)	1040	78	1.9	19,**29**	0.61	ND	—	—
477-5-1 (120–140 cm)	30.7 (37.1)	Diatom. ooze Late Pleist.	ND	2.0	—	ND	1840	83	1.4	19,**29**	0.61	ND	—	—
477-5-cc	32.6 (39.0)	Diatom. ooze Late Pleist.	3.9	2.6	10	0.063(16)	3600	ND	—	—	—	ND	—	—
477-7-1 (124–126 cm)	49.7 (56.8)	Diatom. ooze Late Pleist.	2.8	1.8	8	0.048(21)	860	380	1.1	18,**Ph**	0.24	260	8.1	**16**,24
477-7-1 (132–142 cm)	49.8 (56.9)	Diatom. ooze Late Pleist.	ND	0.9	—	ND	3410	450	1.2	**Ph**,23	0.28	ND	—	—
477-7-2 (14–16 cm)	50.1 (57.2)	Sandy silt, debris flow, Late Pleist.	1.3	0.7	4	0.037(27)	480	180	1.03	19,Ph, 26	0.42	ND	—	—
477-16-5 (58–88 cm)	121.6	Clayey siltstone, ?	ND	0.6	—	ND	87	44	1.0	**19**,23	0.70	ND	—	—
477-17-3 (44–46 cm)	127.9 (133.4)	Silty claystone, ?	1.0	0.8	0	0.083(12)	1000	430	1.03	18,**25**	1.2	ND	—	—
477-20-1 (115–135 cm)	154.2 (160.9)	Silty claystone, ?	ND	0.8	—	ND	100	40	1.1	**19**,25	0.86	ND	—	—
477-20-2 (61–63 cm)	155.1 (161.8)	Silty claystone, ?	1.6	1.0	4	0.034(28)	720	50	1.23	**19**,25	0.83	ND	—	—
477-22-1 (26–28 cm)	172.3 (179.3)	Silty clay, altered, ?	1.6	0.8	7	0.021(47)	410	34	1.14	17,**25**	1.1	ND	—	—
477-23-1 (slick)	185.0 (190.4)	Carbonaceous particulates, ?	14.0	14.0	0	0.012(86)	20	ND	—	none present	—	—	—	—
477A-5-1 (44–46 cm)	191.4 (199.6)	Friable stiltstone, ?	1.2	0.6	6	0.014(69)	3500	400	—	none	—	ND	—	—
477A-9-1 (39–41 cm)	229.4 (237.6)	Sandstone, ?	0.5	0.4	3	0.0001 (8633)	180	14	1.02	19,**25**	1.11	ND	—	—
478-2,3-2,3.6,1 (composite)	8.0	Diatom mud ooze, Late Pleist.	3.9	2.9	9	0.083(12)	500	20	1.73	**19**,29	0.80	ND	—	—
478-2-5 (120–150 cm)	10.7	Diatom, mud ooze, Late Pleist.	ND	2.7	—	ND	3160	108	1.2	16,**19**, 25	0.76	ND	—	—
478-6-3 (120–150 cm)	45.7 (46.2)	Diatom. mud ooze, Late Pleist.	ND	1.4	—	ND	1012	80	1.11	19,**22 29**	0.54	ND		
478-9-3 (110–140 cm)	74.1 (76.8)	Diatom. mud, Late Pleist.	ND	1.5	—	ND	1500	30	1.3	19,27, **29**	1.02	ND	—	—

—continued

Table 1—*continued*

478-12,13-1,2 (composite)	110.0 (114.0)	Diatom. mud ooze, Late Pleist.	3.9	2.4
478-13-2 (120–150 cm)	110.7 (113.9)	Diatom. mud, Late Pleist.	ND	2.2
478-16-4 (120–150 cm)	142.2 (143.5)	Diatom. mud, Late Pleist.	ND	1.0
478-20-4 (108–138 cm)	170.5 (172.3)	Diatom. mud, Late Pleist.	ND	1.1
478-28-4 (120–150 cm)	248.2 (252.2)	Diatom. mud, Late Pleist.	ND	1.8
478-29-1 (57–59,124–126 cm)	251.4 (254.4)	Diatom. mud, Late Pleist.	3.4	2.2
478-29-2 (108–110 cm)	253.1 (255.9)	Dolomitic claystone, Late Pleist.	2.1	1.7
478-29-2 (129–131 cm)	253.3 (256.7)	Dolomitic claystone, Baked, Late Pleist.	1.4	1.4
478-30-1	257.3	Slick, Late Pleist.	—	2.1
478-35-2 (77–79 cm)	300.0 (302.3)	Diatom. mud, Late Pleist.	4.2	2.7
478-35-5 (110–140 cm)	305.1 (307.2)	Dolomitic siltstone, Late Pleist.	ND	0.4
478-40-2 (61–63 cm)	338.1 (343.3)	Dolomitic claystone, Late Pleist.	1.1	1.1
479-9-2 (110–115 cm)	72.2 (74.1)	Diatom. mud, Late Pleist.	ND	2.2
479-19-4 (115–140 cm)	170.1	Diatom. ooze, Late Pleist.	ND	1.8
479-27-4 (120–150 cm)	246.1	Diatom. mud, Late Plioc.	ND	2.3
479-29-5 (114–116 cm)	266.6	Diatom. mud, Late Plioc.	3.0	2.6
479-43-1 (120–140 cm)	393.7 (400.7)	Diatom. mud, Pleist.	ND	1.0
481-2-2 (125–150 cm)	7.6	Diatom. mud ooze, Late Pleist.	ND	2.3
481-11-2 (140–145 cm)	50.4	Wood, Late Pleist.	38.2	38.2
481A-4-2 (110–140 cm)	73.1 (78.8)	Diatom. mud, Late Pleist.	ND	1.5
481A-6-5 (118–120 cm)	96.7	Sand turbidite, Late Pleist.	1.5	1.3
481A-8-7 (0–5 cm)	117.5	Diatom. mud, Late Pleist.	1.6	1.4
481A-12-1 (107–109 cm)	147.6 (148.8)	Silty clay, Late Pleist.	1.5	1.3

—continued

6	0.071(14)	2050	18	2.7	17,**29**	1.17	ND	—	—
—	ND	1490	70	1.2	19,**25**, 27	0.73	ND	—	—
—	ND	1030	30	2.0	19,27, **29**	0.64	ND	—	—
—	ND	660	20	2.0	19,27, **29**	0.38	ND	—	—
—	ND	1450	105	1.04	**16**,19, 27	0.47	ND	—	—
11	0.063(16)	2100	12	3.4	17,**29**	0.50	ND	—	—
3	0.059(17)	240	10	1.07	17,**25**	1.14	ND	—	—
0	0.038(26)	170	8	1.01	**17**,24	3.00	ND	—	—
—	0.045(22)	500	ND	—	—	—	ND	—	—
13	0.059(17)	380	28	1.77	17,22, **29**,31	0.91	40	7.5	**16**,26
—	ND	190	20	1.3	**19**,25	0.20	ND	—	—
0	0.077(13)	680	42	1.07	18,**25**	1.14	ND	—	—
—	ND	1390	78	1.2	16,**19**, 25	0.79	ND	—	—
—	ND	1440	66	0.9	16,19, **22**	0.53	ND	—	—
—	ND	1490	83	0.9	19,**27**	0.29	ND	—	—
3	0.067(15)	680	42	1.07	18,**25**	1.14	ND	—	—
—	ND	780	120	0.9	**Ph**,22, 27	0.20	ND	—	—
—	ND	2550	132	0.97	19,**27**, 29	0.45	ND	—	—
0	ND	490	64	1.6	17,29, **31**	0.88	80	8.6	**16**,26
—	ND	2370	116	1.1	19,27, **29**	0.62	ND	—	—
2	0.071(14)	1060	18	4.0	17,**29**	1.60	12	5.4	16,**30**
2	ND	1410	36	2.5	17,**29**	0.78	45	3.9	16,**30**
2	0.077(13)	2700	74	4.1	16,**29**, 31	0.38	ND	—	—

—continued

Table 1—*continued*

481A-12-4 (55–65 cm)	151.6 (152.8)	Silty clay, turbidite, Late Pleist.	1.4	1.0	4	ND	735	120	1.6	15,Pr, 23,**29**	1.47	70	1.9	**16**,24
481A-13-6 (0–14 cm)	162.0 (163.7)	Sandstone, Late Pleist.	ND	0.6	—	ND	97	37	1.1	**26**	0.29	ND	—	—
481A-14-3 (50–52 cm)	169.0 (172.5)	Silt, Pleist.	1.1	0.8	2	0.053(19)	1010	60	3.2	17,Pr, **29**	1.07	62	3.8	**16**,24
481A-14-4 (2–4 cm)	170.0 (173.5)	Cemented, silt, Pleist.	1.2	0.6	5	ND	490	36	3.3	16,29, **31**	0.40	ND	—	—
481A-14-4 (52–54 cm)	170.5 (174.0)	Siltstone, Pleist.	0.6	0.4	2	0.071(14)	350	18	1.08	18	1.2	ND	—	—
481A-18-1 (27–29 cm)	203.8 (212.4)	Sandy clay, Late Pleist.	1.1	0.9	2	0.071(14)	800	40	2.4	19,**Ph**, 29	0.26	ND	—	—
481A-20-1 (60–62 cm)	223.1 (230.4)	Diatom. mudstone, Late Pleist.	3.5	1.8	14	ND	1740	64	2.8	19,Ph, **29**	0.50	46	3.3	**16**,24
481A-24-5 (110–140 cm)	267.6	Diatom. mudstone, Late Pleist.	ND	0.8	—	ND	520	37	1.4	19,**Ph**, 29	0.47	ND	—	—
481A-25-cc	279.5	Silty claystone, Late Pleist.	1.8	1.1	6	ND	560	26	3.4	17,Ph, **31**	0.45	80	4.8	**16**,22, 28
481A-30-5 (110–140 cm)	325.6	Diatom. mudstone, Late Pleist.	ND	1.4	—	ND	1350	55	1.4	18,21, **Ph**,29	0.29	ND	—	—
30G-1 (Simoneit *et al.*, 1979)	1.0	500 yrBP	2.8	2.5	3	ND	28,000	24	1.5	17,**19**, 29	0.60	30	7.5	**16**,24
30G-1 (Simoneit *et al.*, 1979)	1.8	900 yrBP	2.8	1.8	9	ND	1600	1	3.0	17,**29**	1.20	90	7.8	16,26

Note: ? = age unknown; ND = not determined.

[a]Depth according to DSDP convention; depth calculated upward from the core catcher is given in parentheses (if different).

[b]Data supplied by Shipboard Party (Curray *et al.*, 1982) and Microanalytical Laboratory, Department of Chemistry, University of California, Berkeley.

[c]Based on dry weight of sediment.

[d]Carbon preference index summed from C_{12} to C_{35}; odd-over-even for *n*-alkanes, even-over-odd for *n*-fatty acids.

[e]Dominant homolog is set in bold type.

[f]Pristane-to-phytane ratio (Didyk *et al.*, 1978).

Table 2. Data for kerogens from the Gulf of California

Sample	Sub-bottom depth (m)[a]	Elemental analysis %C[b]	Atomic H/C	Atomic N/C	$\delta^{13}C$ (‰)[c]	ESR Analysis $N(\times 10^{17}$ spins/gC)	Line width (gauss)	g
474-6-5 32–34 cm	46.3 (46.8)	30.8	0.98	0.051	−20.9	1.5	4.6	2.0028
477-5-1 81–91, 94–96 cm	30.4 (36.7)	43.9	1.18	0.060	−20.7	1.1	4.2	2.0027
477-5-cc	32.6 (39.0)	47.6	1.06	0.049	−20.8	2.4	4.1	2.0030
477-7-1 124–126 cm	49.7 (56.8)	28.9	0.94	0.045	−20.8	34	5.1	2.0030
477-7-2 14–16 cm	50.1 (57.2)	25.1	0.42	0.037	−22.4	120	5.1	2.0028
477-17-3 44–46 cm	127.9 (133.4)	34.6	0.61	0.027	−21.7	98	4.7	2.0029
477-20-2 61–63 cm	155.1 (161.8)	36.3	0.51	0.024	−21.2	140	4.2	2.0028
477-22-1 26–28 cm	172.3 (179.3)	41.9	1.12	0.047	−20.4	11	4.4	2.0024
477-23-1 "slick"	185.0 ± 0.7	19.9	0.80	0.013	−21.4	ND[d]	ND[d]	ND[d]
477A-5-1 44–46 cm	191.4 (199.6)	41.8	0.62	0.019	−22.7	27	5.6	2.0028
477A-9-1 39–41 cm	229.4 (237.6)	67.1	0.45	0.011	−23.5	61	7.7	2.0030
478-2-2,3,6; 478-3-1, composited	8.0 to 13.2	42.9	1.05	0.063	−21.1	3.4	4.0	2.0028
478-13-1,2 138–140, 116–118 cm	110.0 (114.0)	44.4	0.89	0.038	−20.7	42	4.1	2.0028
478-29-1 57–59, 124–126 cm	251.4 (254.4)	46.8	0.95	0.048	−20.8	25	5.9	2.0030
478-29-2 108–110 cm	253.1 (255.9)	32.2	0.50	0.045	−20.2	56	6.1	2.0028
478-29-2 129–131 cm	253.3 (256.5)	41.4	0.53	0.037	−20.6	9.2	5.2	2.0029
478-29-2 "slick"	252.7 ± 0.7	59.3	0.64	0.045	−20.9	85	6.4	2.0028
478-30-1 "slick"	257.6 ± 0.7	50.1	0.49	0.052	−20.6	17	5.3	2.0031
478-40-2 61–63 cm	338.1 (343.3)	55.0	0.45	0.031	−20.9	45	4.5	2.0027
479-29-5 114–116 cm	266.6 (266.6)	34.4	1.20	0.046	−19.7	1.5	4.2	2.0028
481-11-2 140–145 cm, wood	50.4 (50.6)	39.0	1.38	0.022	−25.1	ND[d]	ND[d]	ND[d]
481A-12-1 107–109 cm	147.6 (148.8)	27.4	0.87	0.041	−21.1	14	5.1	2.0028
481A-14-3 50–52 cm	169.0 (172.5)	47.8	0.49	0.023	−21.9	170	4.2	2.0030
481A-14-4 2–4 cm	170.0 (173.5)	52.0	0.46	0.021	−21.9	200	4.2	2.0027
481A-14-4 52–54 cm	170.5 (174.0)	51.7	0.49	0.021	−22.0	180	4.1	2.0027
481A-18-1 27–29 cm	203.8 (212.4)	33.2	0.84	0.037	−21.7	65	5.8	2.0028
481A-20-1 60–62 cm	223.1 (230.4)	39.9	0.98	0.050	−21.0	5.1	5.2	2.0031

[a]The subbottom depth is given according to the DSDP convention and in parentheses as it is calculated upward from the core catcher.
[b]Determined after aluminum trichloride digestion and in some cases, heavy liquid separation.
[c]Stable carbon isotope composition recorded in parts per thousand deviation from the PDB Chicago standard.
[d]Not determined, due to insufficient material.

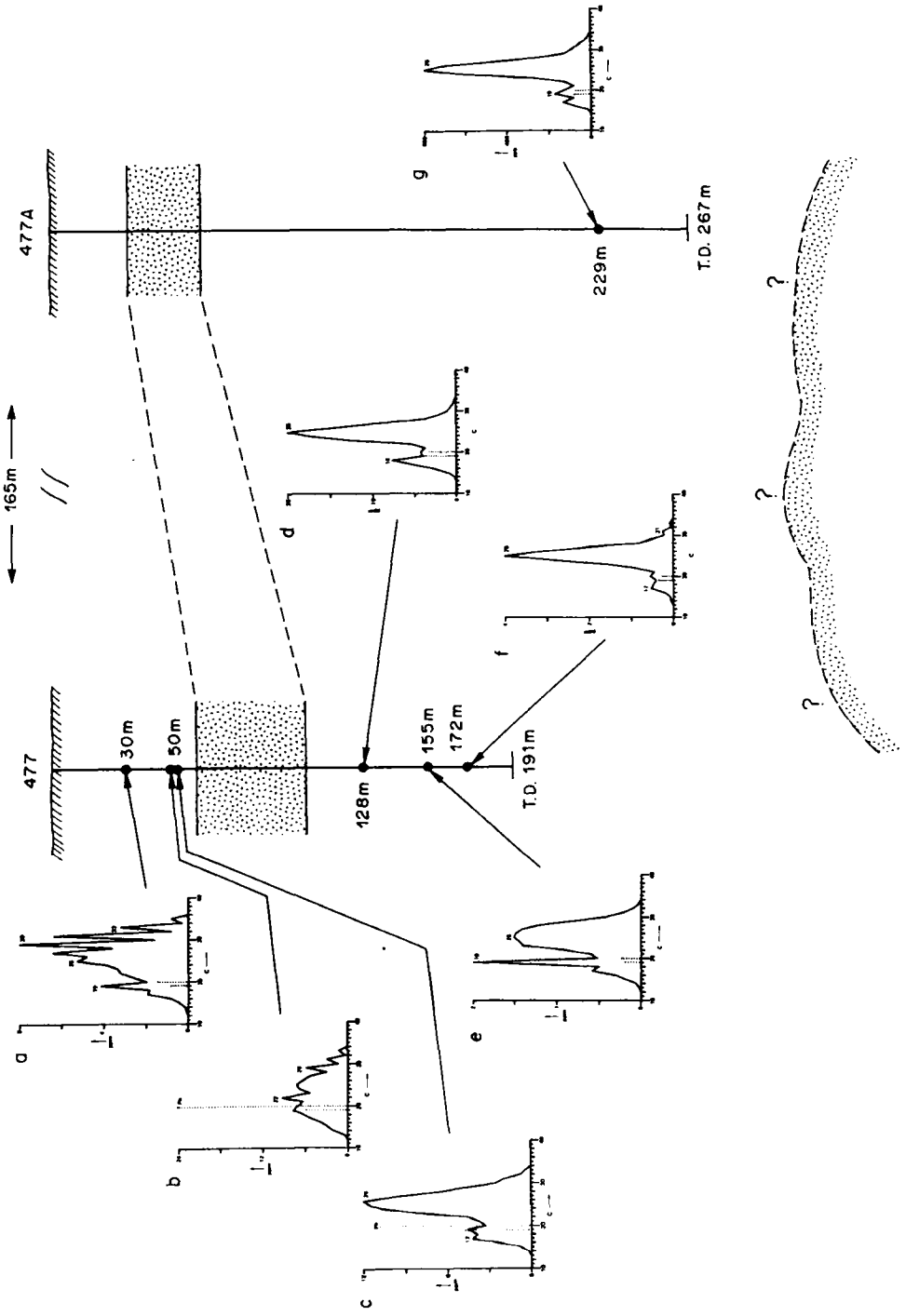

Fig. 6. Distribution diagrams (concentration versus carbon number) for *n*-alkanes of samples from Holes 477 and 477A shown versus sub-bottom depths (...indicates isoprenoids): (a) 477-5-1, 81–91 and 94–96 cm; (b) 477-7-1, 124–126 cm; (c) 477-7-2, 14–16 cm; (d) 477-17-3, 44–46 cm; (e) 477-20-2, 61–63 cm; (f) 477-22-1, 26–28 cm; (g) 477A-9-1, 39–41 cm.

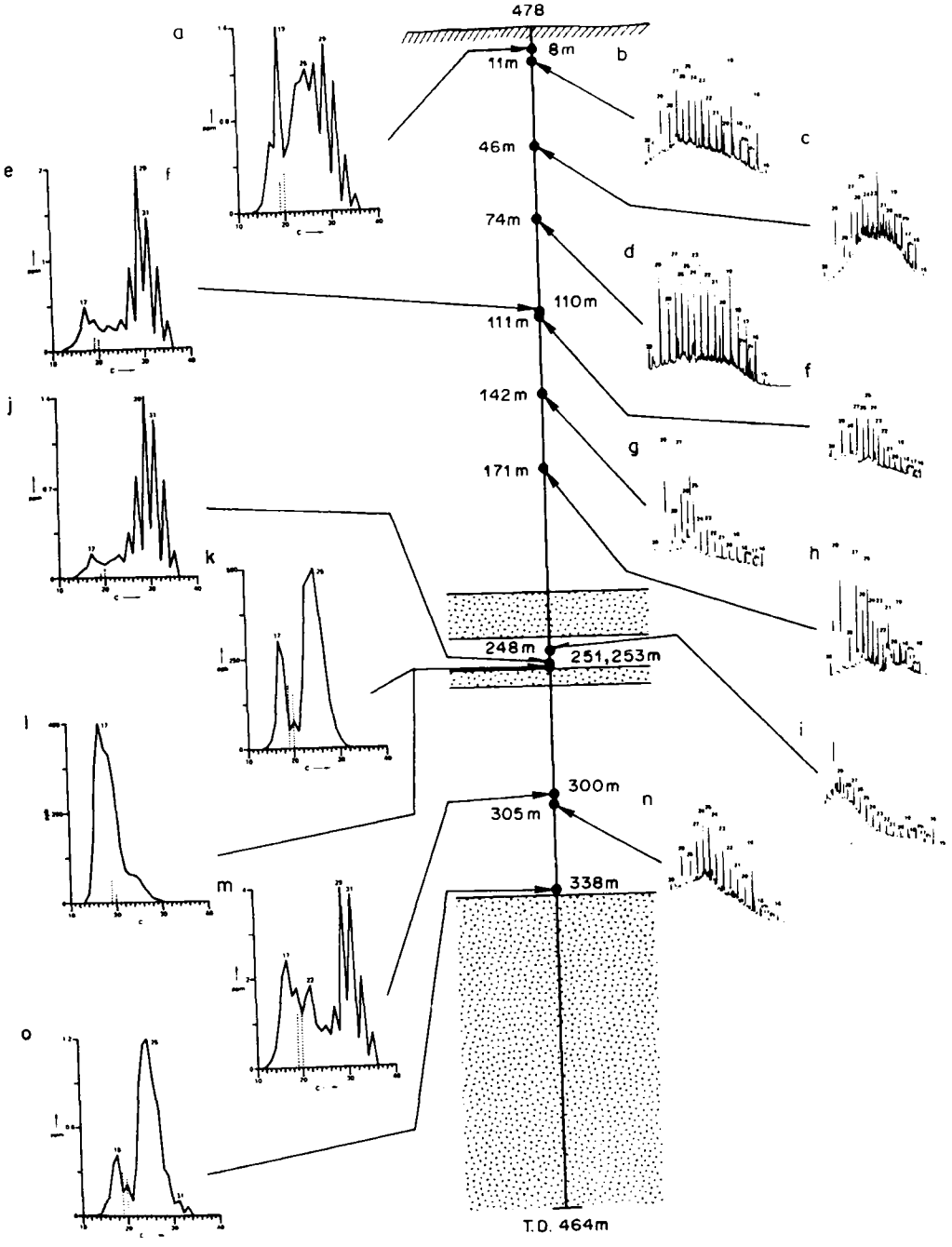

Fig. 7. Distribution diagrams and gas chromatograms for *n*-alkanes of samples from Site 478 shown versus sub-bottom depth (....indicates isoprenoids); numbers on GC traces indicate carbon number of *n*-alkanes, Pr = pristane; Ph = phytane): (a) 478-2/3, composite; (b) 478-2-5, 120–150 cm; (c) 478-6-3, 120–150 cm; (d) 478-9-3, 110–140 cm; (e) 478-13-1/2, 116–118 and 131–140 cm; (f) 478-13-2, 120–150 cm; (g) 478-16-4, 120–150 cm; (h) 478-20-4, 108–138 cm; (i) 478-28-4, 120–150 cm; (j) 478-29-1, 57–59 and 124–126 cm; (k) 478-29-2, 108–110 cm; (l) 478-29-2, 129–131 cm; (m) 478-35-2, 77–79 cm; (n) 478-35-5, 110–140 cm; (o) 478-40-2, 61–63 cm.

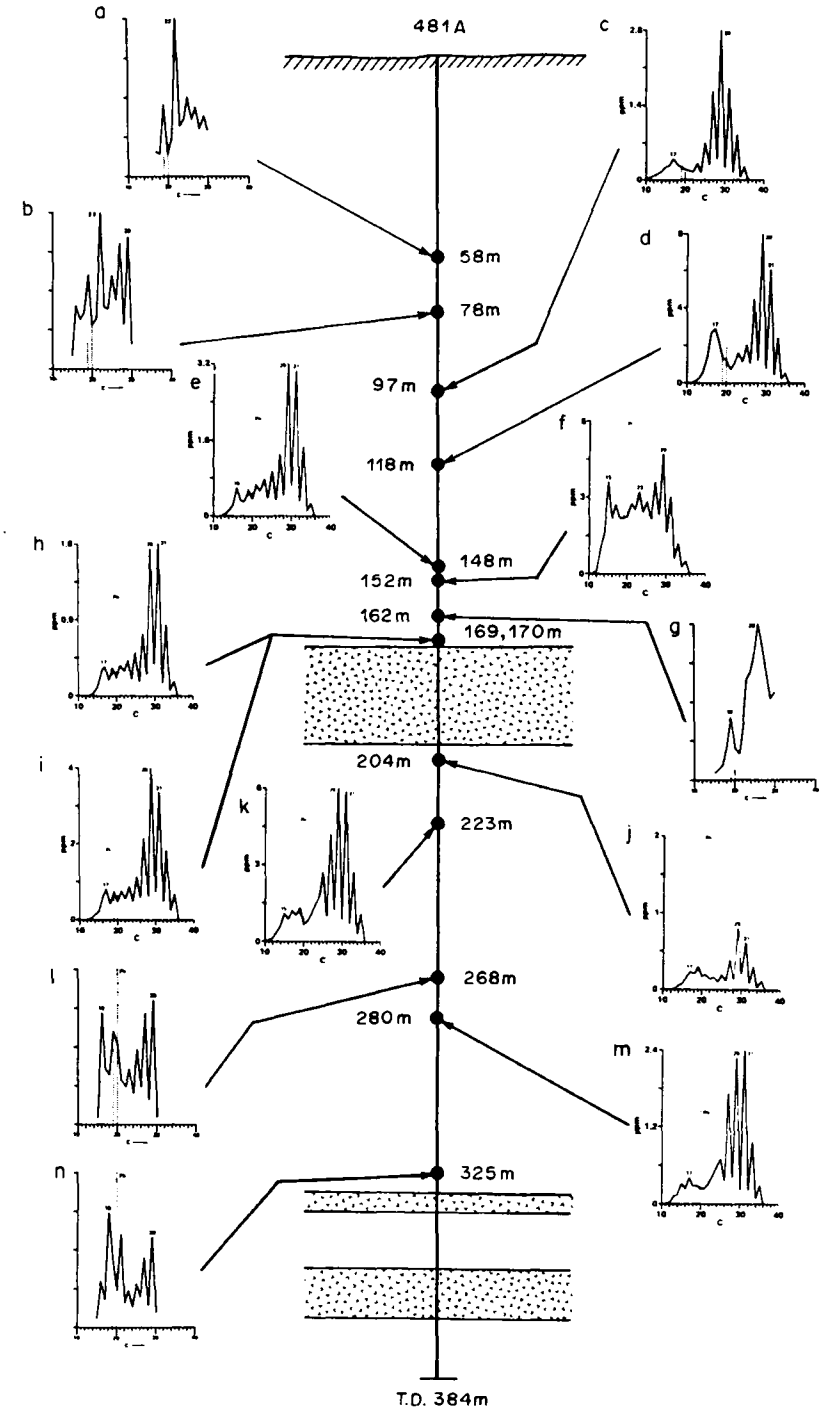

Fig. 8. Distribution diagrams for *n*-alkanes of samples from Site 481 shown versus sub-bottom depth (....indicates isoprenoids): (a) 481-2-2, 125–150 cm; (b) 481A-4-2, 110–140 cm; (c) 481A-6-5, 118–120 cm; (d) 481A-8-7, 0–5 cm; (e) 481A-12-1, 107–109 cm; (f) 481A-12-4, 55–65 cm; (g) 481A-13-6, 0–14 cm; (h) 481A-14-3, 50–52 cm; (i) 481A-14-4, 2–4 cm; (j) 481A-18-1, 27–29 cm; (k) 481A-20-1, 60–62 cm; (l) 481A-24-5, 110–140 cm; (m) 481A-25-cc; (n) 481A-30-5, 110–140 cm.

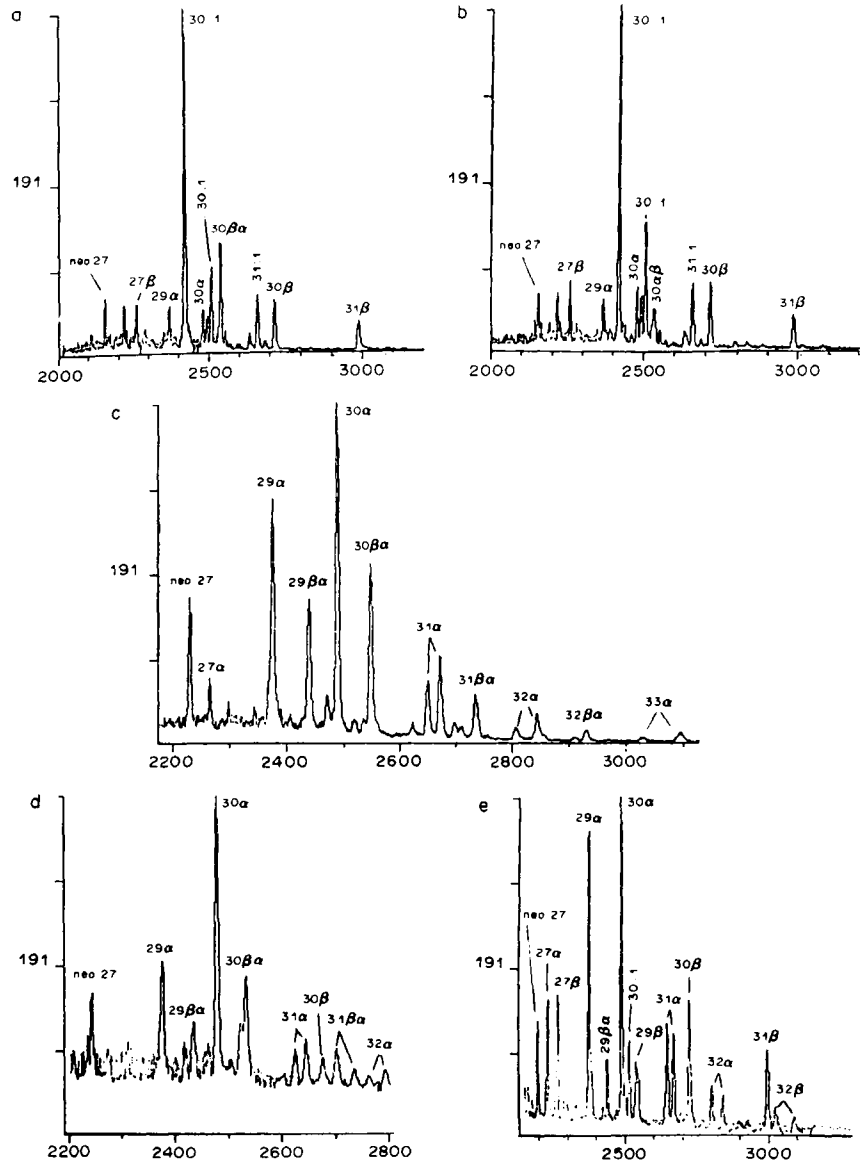

Fig. 9. Selected examples of mass chromatograms (*m/z* 191) indicating the trends of triterpenoid diagenesis and maturation. Numbers indicate carbon skeleton: 1 = olefin; α = 17α(H), 21β(H), βα = 17β(H),21α(H) and β = 17β(H),21β(H) configurations. (a) 481A-25-cc; (b) 481A-8-7, 0–5 cm; (c) 481A-12-4, 55–65 cm; (d) 477-7-1, 124–126 cm; (e) 477-17-3, 44–46 cm.

black shale (DSDP Site 368; Simoneit *et al.*, 1978, 1981). In the latter case, the hydrocarbon distributions near the sill were narrower (C_{12}–C_{20} only).

The molecular markers also show the effects of thermal stress. The triterpenoids of samples close to and below the sill are more mature than the surface samples (e.g. Figs 9d and 9e). They consist primarily of the 17α(H)-hopanes (**II**, 17α), and the extended homologs (>C_{31}) occur with 22S-to-22R ratios of about 1.2. This indicates unusually high maturity for such a Recent sediment. Minor amounts of 17β(H)-hopanes (**II**, 17β) remain and triterpenes are not detectable or are found only in trace amounts (Figs 9d and 9e).

The sesquiterpenoid and diterpenoid residues in the shallow samples occur in trace amounts or as minor aromatized components. The extended tricyclic terpanes (**XII**) are found only as trace components, and they appear to be syngenetic with the triterpanes. As is the case for the shallow immature samples, the C_{27} (marine origin) steranes predominate in the thermally-altered samples, with a significant amount of the 5β(H) stereomers (**XIII**, R = H, 5β) and similar distributions of other analogs as described above (Fig. 10). The C-20 isomerization ratios (Mackenzie *et al.*, 1982b; Seifert and Moldowan, 1979) vary around 10%.

The tetrapyrrole pigments at depth of Site 477 are

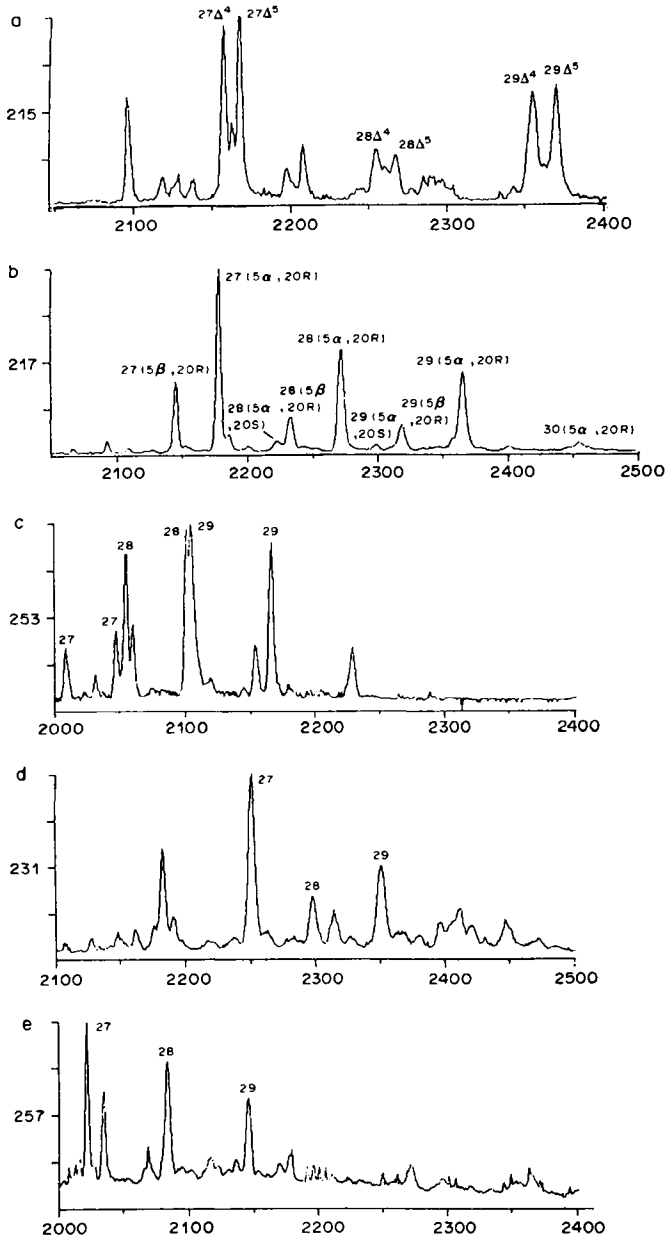

Fig. 10. Selected mass chromatograms illustrating the effect of thermal stress on steroid hydrocarbons. Numbers indicate carbon skeleton, Δ' = double bound position, stereochemistry is summarized in parentheses. Sample 481A-25-cc (a) and sample 477-7-1, 124–126 cm (b–e): (a) *m/z* 215 indicator for sterenes (**XVI**); (b) *m/z* 217, steranes (**XIII**); (c) *m/z* 253, monoaromatic steranes; (d) *m/z* 231, triaromatic steranes (**XV**); (e) *m/z* 257, diasterenes (**XIV**).

mainly nickel porphyrins and sample 477-7-1, 132–142 cm contains nickel, copper and vanadyl porphyrins (Fig. 11; Galimov *et al.*, 1982; Galimov and Kodina, 1983). Samples under high thermal stress have no detectable tetrapyrrole pigments (e.g. 477-16-5, Fig. 11).

The presence of olefins and di-olefins in the deeper samples at this site is due to the high temperatures. These olefins are thermogenic products derived from the protokerogen. The lipid fractions appear to contain large amounts of polysulfide moieties (e.g. S_8, S_7, and S_6), which were probably generated by the hydrothermal activity from organic sulfur and/or H_2S. Polysulfides also occur in euxinic sedimentary environments (e.g. the shallow sediments in the Guaymas Basin and the Southern California Borderland; Simoneit *et al.*, 1979; Simoneit and Mazurek, 1981).

The stable carbon isotope distributions for various bitumen fractions change depending on the level of

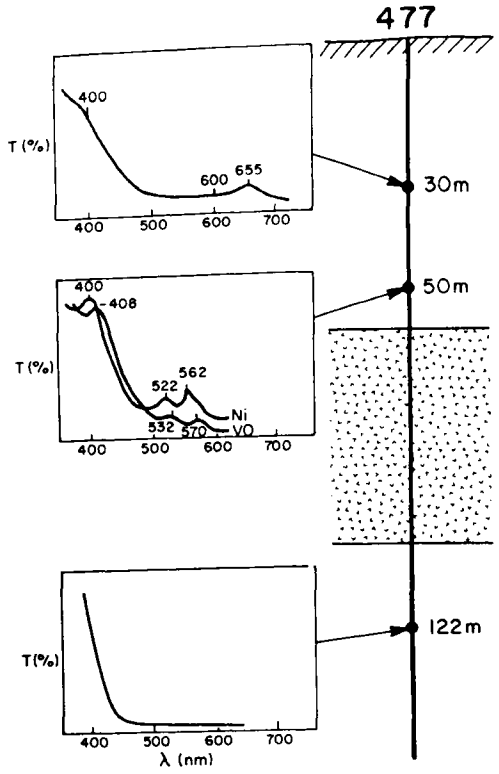

Fig. 11. Tetrapyrrole pigments versus sub-bottom depth in Hole 477: (a) Sample 477-5-1, 120–140 cm, chlorins; (b) Sample 477-7-1, 132–142 cm, Ni and VO porphyrins; (c) Sample 477-16-5, 55–88 cm, no pigments.

thermal stress (Fig. 12; Galimov and Kodina, 1983). In the immature sequence the hydrocarbons are relatively enriched and asphaltenes are depleted in ^{12}C, but in the more mature samples (e.g. 477-16-5) this isotope distribution changes. The $\delta^{13}C$ data vary irregularly and average out (Fig. 12). This indicates a redistribution of carbon isotopes between bitumen fractions due to disproportionation reactions (Galimov and Kodina, 1983). This process generates higher molecular weight condensation products from initially ^{12}C-enriched material (e.g. hydrocarbons), whereas the original hydrocarbons become depleted in ^{12}C due to a kinetic isotope effect that accompanies cracking.

Site 478

The *n*-alkane distributions, hydrocarbon yields, CPI and Pr/Ph ratios for Site 478 are shown in Figs 3 and 7. The lipid distributions in the upper samples of this hole to about 40 m above the major sill are immature, reflecting unaltered biogenic input. The *n*-alkanes $>C_{23}$ are from terrestrial plant waxes (as discussed), and the homologs $<C_{23}$ are of an autochthonous marine origin. The total hydrocarbon yield (Fig. 3) does not show clear maxima near the sill, probably due to the non-uniform lithology and limited sampling.

Sample 478-29-2, 108–110 cm (Fig. 7) is about 1.8 m below composited sample 478-29-1, 57–59 cm, 114–126 cm, and about 0.6–2.9 m above a small sill (~1.5 m thick). The *n*-alkanes appear altered ($>C_{21}$), with a remnant microbiological imprint $<C_{20}$. Sample 478-29-2, 123–131 cm, which is 5 cm from the contact of the small sill, is in the hydrothermally-altered zone. The *n*-alkanes confirm this by their low concentration and very narrow distribution, similar to that of the intruded Cretaceous shales (Simoneit *et al.*, 1978, 1981).

These hydrothermally-altered samples do not contain significant amounts of molecular markers (e.g. triterpanes) but have high concentrations of sulfur (S_8, etc.) and some minor polycyclic aromatic hydrocarbon series. The triterpanes and other lipids appear to have been removed by hydrothermal circulation and/or by thermal conversion to other products (e.g. aromatics).

Site 481

The sediments of Hole 481A were intruded by two dolerite sills. However, the lipids from the samples are essentially unaltered, reflecting their biogenic origin (Figs 4 and 8). The hydrocarbon yields, CPI

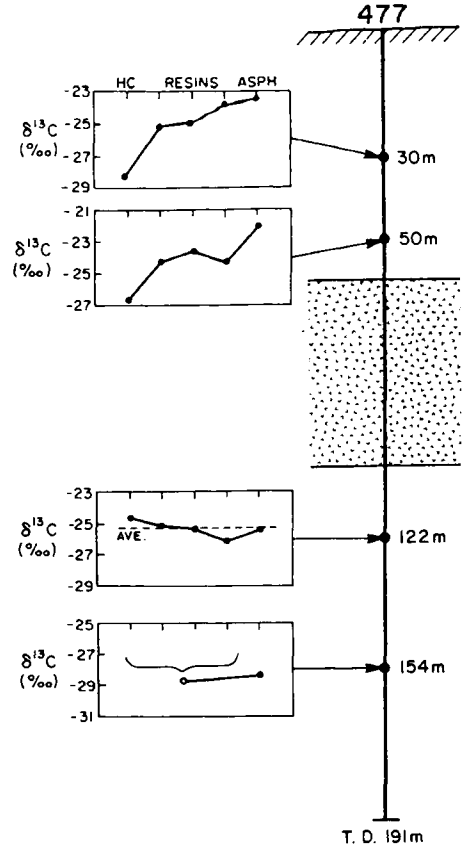

Fig. 12. Effects of thermal stress on the stable carbon isotope distributions of various bitumen fractions (hydrocarbons, resins, asphaltenes; Galimov *et al.*, 1982) at Site 477.

and Pr/Ph show no obvious trends versus depth and near sills (Fig. 4), indicating that thermal effects due to the intrusions were minor.

Sample 481A-12-1, 107–109 cm (Fig. 8) is about 25 m above the upper sill complex (Einsele *et al.*, 1980). The *n*-alkane distribution is essentially the same as that in shallow samples. Phytane is predominant, where the variability in concentrations is probably the result of minor differences in paleoenvironmental conditions. Sample 481A-12-4, 55–65 cm is about 22 m above the upper sill complex. Its composition for the *n*-alkanes and *n*-fatty acids differs from shallower samples. The even-carbon-number alkanes represent a significant proportion of the homologous series; the odd-carbon-number fatty acids are also quite high (Simoneit and Philp, 1982). Pristane is the dominant isoprenoid hydrocarbon. This may represent some thermogenic contribution to the natural background lipids. The distribution closely resembles others in the intruded Cretaceous shale sequences (Simoneit *et al.*, 1978, 1981), which is supported further by the two next-lower samples, containing essentially no thermogenic lipids.

Two samples (481A-14-4, 2–4 cm and 481A-14-4, 52–54 cm) which are relatively close to the sill (Fig. 8, about 5 and 50 cm) exhibit the same biogenic fingerprints as observed in the shallow samples. The *n*-alkanes are dominated by terrestrial plant wax ($>C_{23}$), with minor autochthonous microbial constituents; the *n*-fatty acids also contain both of these source components (Simoneit and Philp, 1982). Two explanations for the presence of these immature, unaltered lipids close to the sill are proposed. First, the true *in situ* distance of the samples from the sill contact may have been greater because of sediment loss during drilling. Second, the section above the sill (a megaturbidite; Fig. 4), which includes these samples, may have been emplaced on a flow of basalt after cooling. This second suggestion, however, is not supported by the data for samples below the sill, since they too, are essentially unaltered.

However, at about 5 cm (or 3.5 m; sample 481A-14-4, 52–54 cm; Table 1) above the sill, the hydrocarbon distribution is heavily altered. The *n*-alkanes range from C_{13} to C_{29}, with a maximum at C_{18} and essentially no carbon-number predominance. This distribution reflects the effects of thermal stress, as confirmed by the presence of various olefins, and a large amount of sulfur. The major olefins are the *n*-alk-1-enes ranging from C_{14} to C_{26}, with a strong, even-carbon-number predominance and maximum at C_{18}.

Samples below the major sill complex, and more than 50 m above the minor sills at depth have distributions of *n*-alkanes which are essentially identical (Fig. 8). Terrestrial-plant-wax components predominate, and there are minor autochthonous marine lipids. These distributions are also similar to those just above the sill complex and those in the shallow samples. Thermogenic lipids are not evident.

The molecular markers of the lipids from Hole 481A show limited effects of thermal maturation, and most are immature. Diterpenoids and sesquiterpenoids are present. They consist of dehydroabietic acid (**I**), cadalene (**VII**), dehydroabietin (**IX**), retene (**X**, R = CH_3), simonellite (**XI**, R = CH_3), 1-methyl-7-ethylphenanthrene (**X**, R = H), and norsimonellite (**XI**, R = H). The triterpenoids of the deepest sample (Fig. 9a) consist mainly of 17β(H)-hopanes (**II**), *iso*-hop-13(18)-ene (**VI**), hopenes and moretanes. Their distribution is essentially identical to that for the shallow sample from Section 481A-8-7 (Fig. 9b) and represents immature markers in the early stages of diagenesis. The triterpenoids of the samples close to the sill complex are more mature (e.g. Fig. 9c), with a dominance of 17α(H)-hopanes (**II**) and 17β(H)-moretanes (**V**) and essentially no triterpenes. These distributions approach the mature patterns at Site 477 (e.g. Figs 9d and 9e). Based on the immature nature of deeper samples, there appears to have been a weak but definite thermal effect on the molecular markers in the lipids of the sediments near the upper sill complex. The sterane distributions support the proposed lipid alterations caused by thermal effects near the upper sill complex. Sterenes (e.g. **XVI**) predominate (e.g. Fig. 10a) in progressively deeper samples, while steranes (**XIII**), diasterenes (**XIV**) and aromatic steranes (e.g. **XV**) occur closer to the sills. Increasing thermal maturation is further indicated near sills by the appearance of 5α, 14α, 17α(H)-steranes and the C-20 isomerization ratio approaches 10%.

The tetrapyrrole pigments in samples from Hole 481A are comprised of nickel porphyrins and no pigments are detectable near sills (Galimov *et al.*, 1982; Galimov and Kodina, 1983).

Kerogen Analyses

In this section the elemental composition, stable carbon isotope and electron spin resonance data are discussed first, followed by the pyrolysis data. Analytical data for the kerogens are summarized in Table 2.

Bulk chemistry

Atomic H/C ratios and $\delta^{13}C$ values for the shallowest samples at the five sites listed in Table 2 average 1.16 and −21.5‰, respectively. These values indicate a type II kerogen composed largely of marine organic matter (Tissot and Welte, 1978; Galimov, 1980). This observation is confirmed by Curie point pyrolysis (this paper) and agrees with results obtained by Kendrick (1982).

Figure 13 shows that the atomic H/C ratios decrease near the dolerite sills at Sites 477, 478, and 481. This is due to the thermal liberation of water, light hydrocarbons and heavy bitumen. Concurrent with the loss of these hydrogen-rich volatiles is a decrease in atomic N/C ratio, presumably due to the elimination of ammonia (Rohrback *et al.*, 1983).

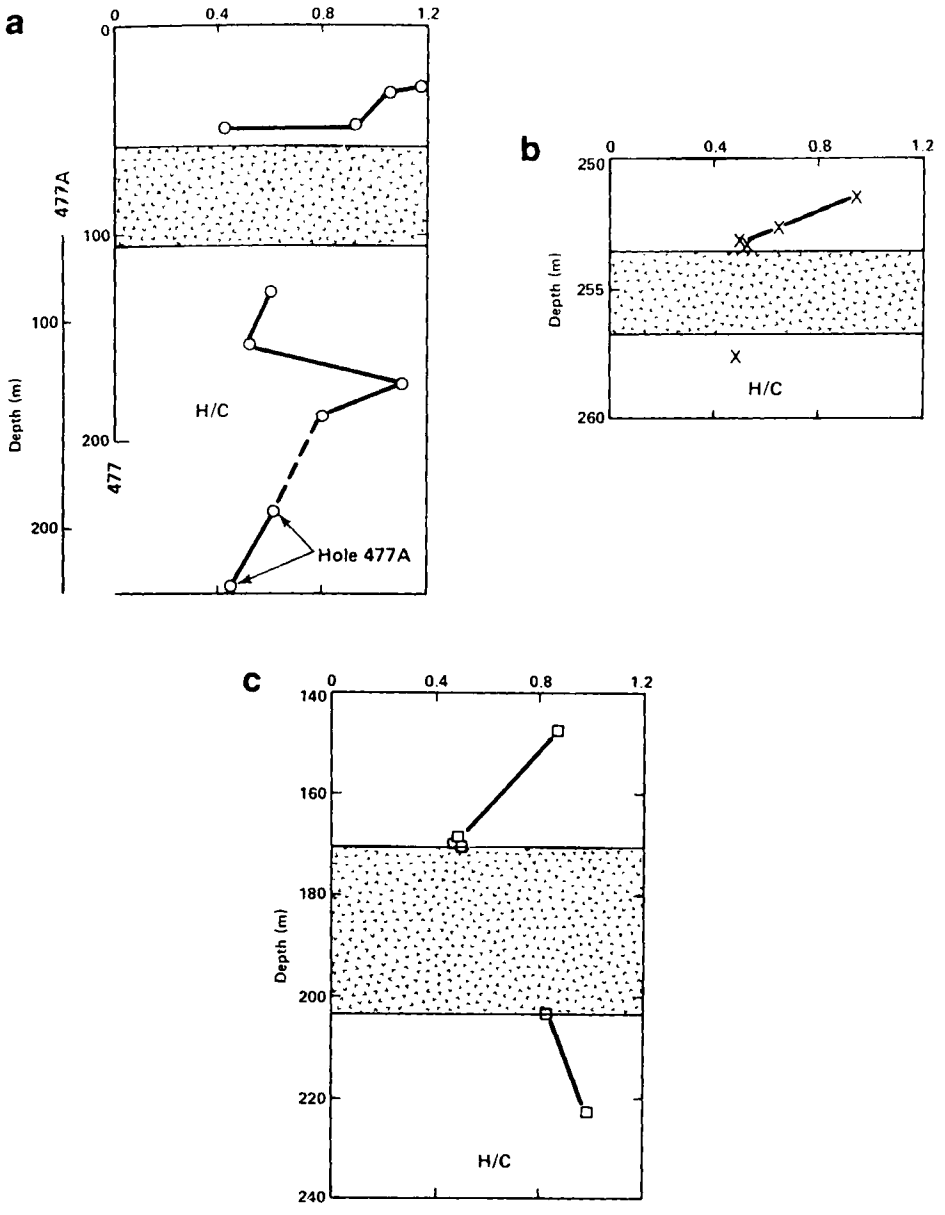

Fig. 13. Plots of atomic H/C data for kerogens versus sub-bottom depth in the vicinity of dolerite sills. (a) Site 477; (b) Site 478; (c) Site 481.

With increasing alteration, ESR spin density and line width pass through maxima (Jenden *et al.*, 1982). The spin density maximum is caused by the competing processes of free radical generation by homolytic cleavage of alkyl side chains and free radical elimination by electron pairing (Austen *et al.*, 1966; Ishiwatari *et al.*, 1977; Ho, 1979; Peters *et al.*, 1981). The line width maximum has been observed in several other studies, but is not well understood (Pusey, 1973; Durand *et al.*, 1977; Morishima and Matsubayashi, 1978; Peters, 1978; Baker *et al.*, 1978; Marchand and Conard, 1980; Peters *et al.*, 1981; Jenden, 1983). ESR *g*-values fall between 2.0027 and 2.0031 and do not vary with maturity. This may be due to the presence of humic acids which could easily mask a small decrease (Jenden *et al.*, 1982).

Significant differences in the nature of the organic matter at Sites 477, 478, and 481 seem unlikely because the sites are all located in the Guaymas Basin within 25 km of one another. Nevertheless, different responses to thermal stress are apparent.

For instance, Fig. 14, which shows atomic N/C versus atomic H/C, indicates that kerogen from Site 478 has lost comparatively less nitrogen than kerogens from Sites 477 and 481. The atomic N/C ratios for highly-altered kerogens at Sites 477 and 481 cluster between 0.025 and 0.011. A similar range of N/C ratios was observed by Simoneit *et al.* (1981) for

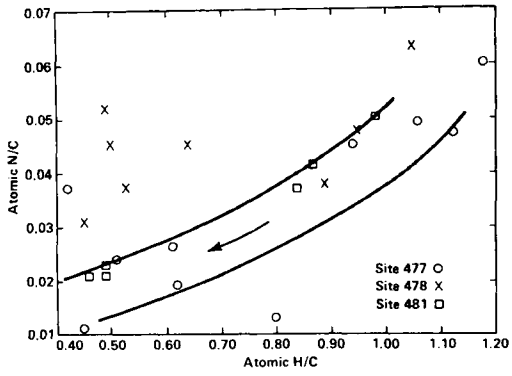

Fig. 14. Plot of atomic N/C versus atomic H/C data for kerogens from Sites 477, 478 and 481. The arrow indicates the general maturation path for kerogens from Sites 477 and 481.

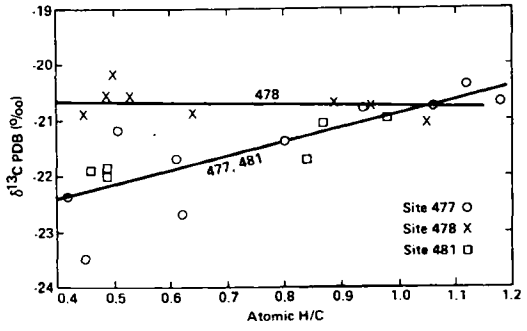

Fig. 15. Plot of $\delta^{13}C$ versus atomic H/C data for kerogens from Sites 477, 478 and 481 (Site 478 data falls on a different correlation line).

Cretaceous sediments recovered adjacent to diabase sills in the Eastern Atlantic. In contrast, the atomic N/C ratios of highly-altered kerogen from Site 478 range from 0.031 to 0.052.

Other differences are also apparent. At Sites 477 and 481, $\delta^{13}C$ values decrease by 1 to 1.5‰ as the dolerite sills are approached. However, little or no change in $\delta^{13}C$ is observed at Site 478. This behavior is illustrated in Fig. 15 which shows a plot of $\delta^{13}C$ versus atomic H/C.

Thermal alteration experiments (Ishiwatari *et al.*, 1977; Peters *et al.*, 1981) and analysis of regional metamorphic effects (McKirdy and Powell, 1974; Hoefs and Frey, 1976) have shown that small increases in $\delta^{13}C$ from a few tenths of a permil to 1.5‰ or more may accompany kerogen maturation into the dry gas zone. Simoneit *et al.* (1981) found an increase of 2–4‰ in kerogen $\delta^{13}C$ as a result of diabase intrusions in Cretaceous black shales. These increases in $\delta^{13}C$ during kerogen maturation are attributed to the production of isotopically light hydrocarbons by cracking reactions. The carbon isotope behavior of kerogen from Site 478 is consistent with these findings, whereas the distinct decreases in $\delta^{13}C$ observed at Sites 477 and 481 are not.

Finally, ESR spin density, *N*, for kerogens appears to show a different response to thermal stress at the three sites. *N* is plotted against atomic H/C for Sites 477, 478, and 481 in Fig. 16. The spin concentration of kerogen from Site 478 is generally lower than that of kerogen from Sites 477 and 481 and follows a different maturation path. Immature kerogens at both sites have spin densities of $1–10 \times 10^{17}$ spins/g C. Kerogens from Sites 477 and 481, however, show a slow initial increase in spin density with increasing maturity followed by a sharp maximum of 200×10^{17} spins/g C at an H/C of 0.45. In contrast, kerogen from Site 478 shows a sharp increase in spin density with increasing maturity followed by a broad maximum of 85×10^{17} spins/g C at an H/C of 0.64. Simoneit *et al.* (1981) observed a spin density maximum of 80×10^{17} spins/g kerogen at an atomic H/C value of 0.61 for altered sediments from the Eastern Atlantic.

The reason for the differences between Site 478 and Sites 477 and 481 is unclear. At all three sites, Quaternary diatomaceous oozes and turbidites overlie basaltic crust less than or equal to 260,000 years old (Curray *et al.*, 1982). Little or no evidence exists for major differences in the type of organic matter deposited (Simoneit *et al.*, 1984). The sediments at Site 478 are located approximately 12 km from the present spreading axis and may be somewhat older than the active rift sediments from Sites 477 and 481. However, of more interest is the fact that four of the five altered samples from Site 478 were recovered near a sill only 3 m thick. The samples from Sites 477 and 481 were recovered near sills ten times thicker. The different maturation behaviors might therefore reflect more prolonged heating and hydrothermal

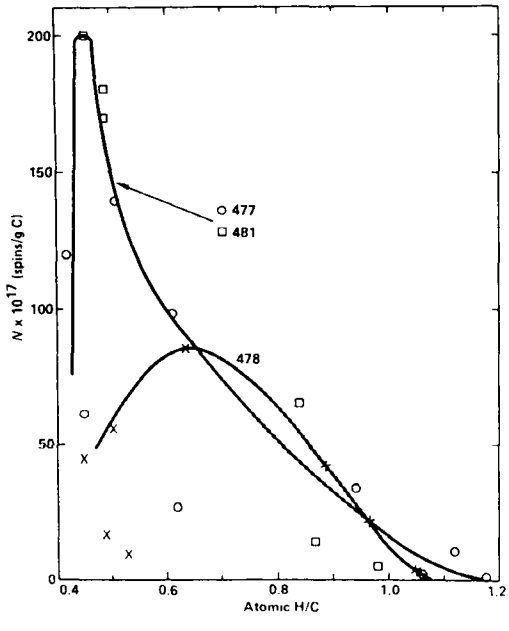

Fig. 16. Plot of ESR spin density (*N*) versus atomic H/C for kerogens from Sites 477, 478 and 481.

circulation in the case of the samples recovered from Sites 477 and 481. Unfortunately, optical measurements of maturation, which might have shed some light on this possibility, were not conducted.

In any case, the maturation behavior, and more specifically, the unusual $\delta^{13}C$ trends at Sites 477 and 481, appear to reflect the chemical and isotopic heterogeneity of very young organic matter. Abelson and Hoering (1961), Galimov (1974), and Monson and Hayes (1982) have clearly demonstrated that biochemical molecules are isotopically heterogeneous. Moreover, young sediments typically contain appreciable amounts of humic and fulvic acids, which are chemically and isotopically distinct from coexisting kerogen (Nissenbaum and Kaplan, 1972). Simoneit *et al.* (1979) found that humic acids comprise 20% of the organic matter in surface sediments from the Guaymas Basin. The situation may be further complicated by the presence of terrestrial as well as marine organic matter in the Guaymas Basin cores (Gilbert and Summerhayes, 1982). Taken together, the present results suggest more complete elimination of a nitrogen- and ^{13}C-rich component at Sites 477 and 481 than at Site 478. The chemical and isotopic heterogeneity of recently deposited organic matter may cause a more complex response to thermal stress than would be expected of a kerogen which has already undergone an extensive period of early-diagenetic maturation.

Pyrolysis

This section compares the pyrolysis products of kerogens from shallow samples at each site. In addition, the pyrograms of the kerogens isolated from the down-hole samples are discussed in detail, with emphasis on the effects of the intrusions.

(I) *Shallow Samples from Sites 474, 477, 478, and 479:*

The similarity of the pyrograms for the shallow samples shows that the organic material deposited at all four sites is very similar (Simoneit and Philp, 1982; Peters and Simoneit, 1982). These pyrograms are comparable to that of a kerogen isolated from a diatomaceous ooze (from Walvis Bay, Namibian Shelf, S.W. Africa) (Simoneit and Philp, 1982). Thus, the bulk organic matter deposited at the Gulf of California sites is predominantly marine and lacks a significant contribution from higher plants (Peters and Simoneit, 1982; Simoneit and Philp, 1982). This is in contrast to the lipid results, where a plant wax component is present.

The major features of the pyrograms, which are similar to that of 477-5-cc shown in Fig. 17 can be summarized as follows:

(1) They show a predominance of *n*-alkene/alkane doublets in the range C_{10} to C_{21} or C_{22}, with relatively minor amounts of higher homologs above C_{22}. The alkene in each doublet generally dominates the corresponding alkane. The complex "humps" of unresolved components obscure any marked even/odd predominance of these doublets. Unlike the isoprenoids, normal paraffins and olefins can originate from all kinds of lipids, and hence, these products can only be used to give an indication of relative amounts of marine versus terrestrial material (van de Meent *et al.*, 1980). However, the relatively low concentration of aliphatic products in the higher-carbon-number range probably reflects the low abundance of long-chain structures generally encountered in the macromolecular organic matter (protokerogen) of aquatic ecosystems or possible precursors from other terrestrial sources.

(2) Prist-1-ene is prominent in each pyrogram and generally is twice as concentrated as the C_{17} doublet. The mass spectrum of the prist-1-ene in these samples corresponds to that identified by Larter *et al.* (1979) as the major pyrolysis product of Messel shale kerogen. Prist-1-ene is common in the pyrolysates of surface sediments from environments extremely rich in phytoplankton. This indicates rapid biotransformation of the phytol moiety on chlorophyll into the pristene precursor (van de Meent *et al.*, 1980). Prist-1-ene is common in almost all pyrograms of geological samples reported in the literature. In the pyrogram of the Site 474 sample, prist-1-ene and prist-2-ene occur in approximately a 1 : 1 ratio. The presence of prist-2-ene is not widely documented and it only appears in samples of relatively recent geological age. This suggests the possibility of using the prist-1-ene/prist-2-ene ratio as an early maturation indicator for samples composed of similar source material.

(3) The pyrograms in Figs 17a, 18a, 18b, 19a and 19d exhibit complex humps of unresolved components underlying the alkene/alkane doublets. The humps have two maxima, the first in the C_{18} to C_{20} region appears to consist of polar material (possibly phenolic). The peaks on the second hump in the C_{28}–C_{30} region presumably represent sterane and triterpane derivatives as observed by Gallegos (1975) and Philp *et al.* (1978), and differences in relative concentrations of individual components probably reflect differences in source material and/or the environmental conditions during deposition. Cupy–GC–MS of these samples provided partial mass spectra to support the identification of the steranes and triterpanes. Their relative concentrations were low, as was the quality of their mass spectra. However, a combination of this data with the relative retention times support these tentative identifications.

(4) Comparing these pyrograms with those obtained from immature terrestrial-type kerogens or lignite (van de Meent *et al.*, 1980) confirms the essential absence of higher plant contributions to the shallow Guaymas Basin kerogens. Unlike the latter, kerogens from sediments rich in terrestrial higher plant detritus produce significant amounts of alkyl- and methoxyphenols. Wax residues from higher

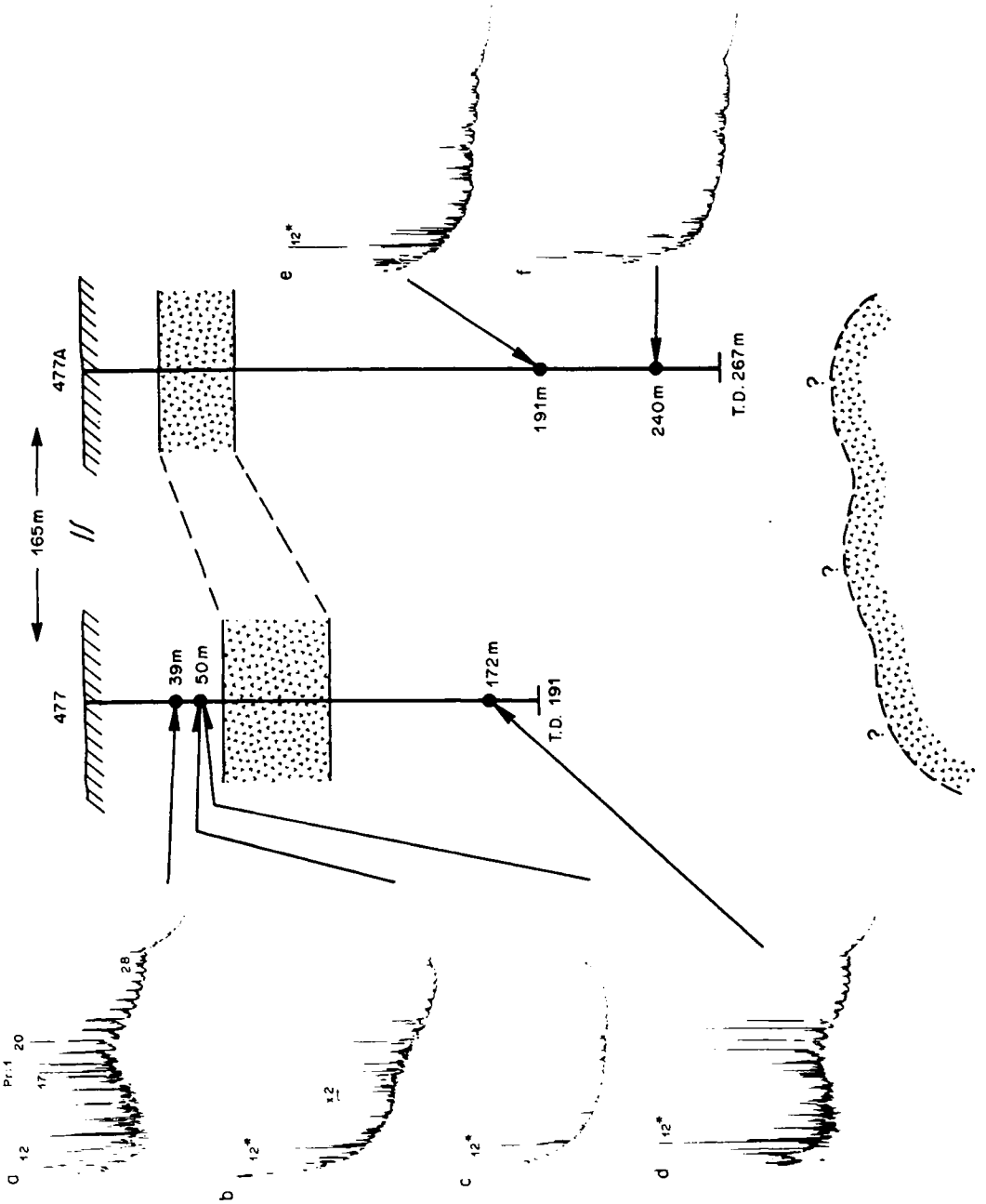
477A
477
165m
39m
50m
172m
T.D. 191
191m
240m
T.D. 267m
a
b
c
d
e
f
12*
Pr:1
20
17
28
?
?
?

plants occur in the pyrolysates as long-chain alkanes with odd and alkenes with even carbon-number predominances, respectively. Phenol humps and long-chain alkene/alkanes are found in only minor amounts in some of these types of kerogens.

(II) *Effect of burial and sill intrusions on kerogen:*

(i) *Holes 477 and 477A.* Sample 477-7-1, 124–126 cm is the first kerogen examined in this study that shows the effects of a dolerite intrusion. A characteristic feature in the pyrograms of all kerogens thought to have been affected by sill intrusions is the presence of a complex multiplet of components in the n-C_{12} region (GC elution) of their pyrograms. These appeared to be aromatic, based on low level, inconclusive Cupy–GC–MS data. The abundance of the alkene/alkane doublets for altered samples decreases compared to unaltered kerogens. Although prist-1-ene is still present, the relative abundance of the unresolved complex hump is reduced in the pyrograms. The "natural" pyrolysis induced by the sill intrusions removed much of easily pyrolyzable material responsible for the complex pyrograms of the shallow samples. It may also have altered the kerogen structure, such that subsequent Cupy-GC produces the complex, but characteristic, multiplet in the n-C_{12} region.

The effects of the sill intrusion are more distinct in the kerogen pyrogram for sample 477-7-2, 14–16 cm (Fig. 17c). The multiplet of peaks in the n-C_{12} region is the most abundant feature of the pyrogram. Components in the C_{18}–C_{20} region are present only in relatively minor quantities. None of the other features described for the pyrograms of shallow samples are present. The alkene/alkane doublets, prist-1-ene and prist-2-ene are absent, and the pyrogram is devoid of any complex hump of unresolved components. The structural source of these traces of volatilizable compounds is unknown.

Sample 477-17-3, 44–46 cm was taken approximately 25 m below the bottom of the sill (cf. Fig. 2). The kerogen pyrogram is virtually identical to that of sample 477-7-2, 14–16 cm (Fig. 17c) which is from 0.8 to 7.6 meters above the sill. A comparison of kerogen pyrograms from similar distances above and below the sill, suggests that those below have been affected slightly more by the heat than those above. Two explanations are: Heat transfer laterally and through the underlying sediments from the sill is more efficient, or the underlying sediments are affected both by the heat from the sill and additional heat flow from depth (Curray *et al.*, 1979, 1982; Einsele *et al.*, 1980). A firm conclusion on this matter cannot be drawn from these data.

There is a progressive depletion with depth of pyrolysis products that can be generated from samples below the sill. Sample 477-22-1, 26–28 cm (Fig. 17d) has a significant pyrolysate of unknown compounds. Multiplets in the n-C_{12} region represent the major peaks of the pyrogram of sample 477A-5-1, 44–46 cm (Fig. 17e). Relatively small amounts of alkene/alkane doublets and broad peaks, tentatively identified as phenolic-type compounds from Cupy–GC–MS data, also occur in the region above C_{20}. These phenolic type compounds may be present in pyrograms of shallow samples, but are not easily observed because of the much higher abundance of the alkene/alkane doublets. Their low abundance in this sample precluded the acquisition of high quality mass spectra.

Sample 477A-9-1, 39–41 cm is the deepest from this site (Fig. 17f). The pyrogram of this kerogen does not differ significantly from that described for sample 477A-5-1, 44–46 cm. Again, it is proposed that this organic matter has been altered by high heat flow from depth, and not from the sill (Curray *et al.*, 1979, 1982; Einsele *et al.*, 1980).

(ii) *Site 478.* Cores recovered at this site range from 0 to 464 m sub-bottom and dolerite sills intruded the section at 230 and 255 m (Fig. 3). Composite sample 478-2-2 (2–5 cm), -2-6 (102–104 cm), -3-1 (19–21 cm) has a kerogen pyrogram (Fig. 18a) essentially identical to the other shallow samples described above. Sample 478-29-1/2, composite (Fig. 18b) is essentially unaltered and sample 478-29-2, 108–110 cm, approximately 0.4–3 m from the sill, shows some thermal effects from the intrusion. In the pyrogram (Fig. 18c) the unresolved complex humps are small; prist-1-ene predominates over prist-2-ene, and the alkene/alkane doublets are reduced. In addition, a complex mixture of components is present in the C_{17}–C_{21} region.

Sample 478-29-2, 129–131 cm is 0.2 to 2.8 m from the sill contact, and the kerogen pyrogram confirms more extensive thermal alteration than in sample 478-29-2, 108–110 cm. The predominance of the multiplet in the n-C_{12} region of the pyrogram suggests extensive alteration due to the intrusion. The relative intensity of the alkene/alkane doublets has been further reduced. The complex mixture in the C_{17}–C_{22} region is still evident and similar to that in the pyrogram of 478-29-2, 108–110 cm.

The organic matter in Section 478-30-1 was sampled as a hydrophobic slick on the interstitial water of split cores. It was characterized as amorphous activated carbon and represents the *in situ* spent kerogen (Simoneit, 1982d; Curray *et al.*, 1982). This carbonaceous slick also reflects thermal stress from the sill (cf. Fig. 18d). The amount of pyrolyzable material is reduced, but the characteristics of a thermally altered sample remain in the pyrogram. The alkene/alkane doublets are absent, and the appearance of a series of well-defined humps of polar material is observed in the C_{17}–C_{22} region of the pyrogram.

Sample 478-40-2, 61–63 cm occurs about 340 m sub-bottom, eliminating any possibility of alteration of the organic material by the sill at 255 m. Most of the alteration is probably due to the major dolerite sill immediately below the sample. The pyrogram (Fig. 18e) is similar to that of the slick described above (Fig. 18d). The multiplet in the n-C_{12} region is

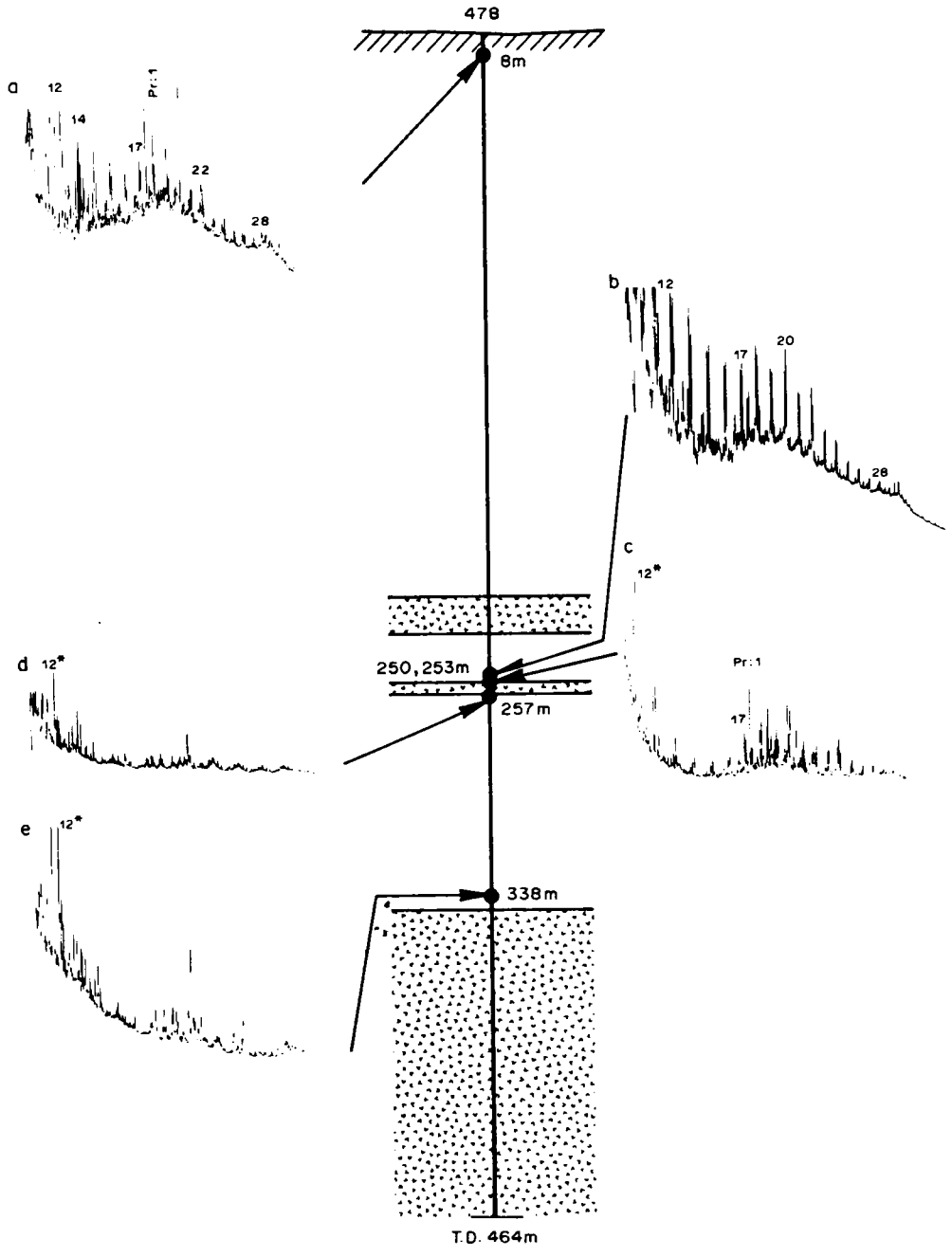

Fig. 18. Examples of Cupy–GC traces for kerogens from Site 478 shown versus sub-bottom depth: (a) 478-2/3-2,6,1, composite; (b) 478-29-1/2, composite; (c) 478-29-2, 108–110 cm; (d) 478-30-1, slick; (e) 478-40-2, 61–63 cm.

present, and the alkene/alkane doublets and prist-1-ene are absent. Phenolic-type humps, tentatively identified as more polar phenolic compounds, occur in the C_{12}–C_{22} region.

(iii) *Site 481.* The shallowest sample analyzed from this hole occurs at a depth of 147.5 m; therefore, no direct comparison has been made with shallow samples from the other sites. Changes in the pyrograms with increasing sample depth, however, show that alteration was caused by the intrusions and not by burial maturation.

Sample 481A-12-1, 107–109 cm is from about 25 m above the sill complex (170.5–203 m sub-bottom; cf. Fig. 4). The kerogen pyrogram exhibits early signs of thermal alteration (Fig. 19a). The multiplet is weakly developed in the n-C_{12} region and the complex humps in pyrograms of shallow samples from other sites are essentially absent. The pyrogram is domin-

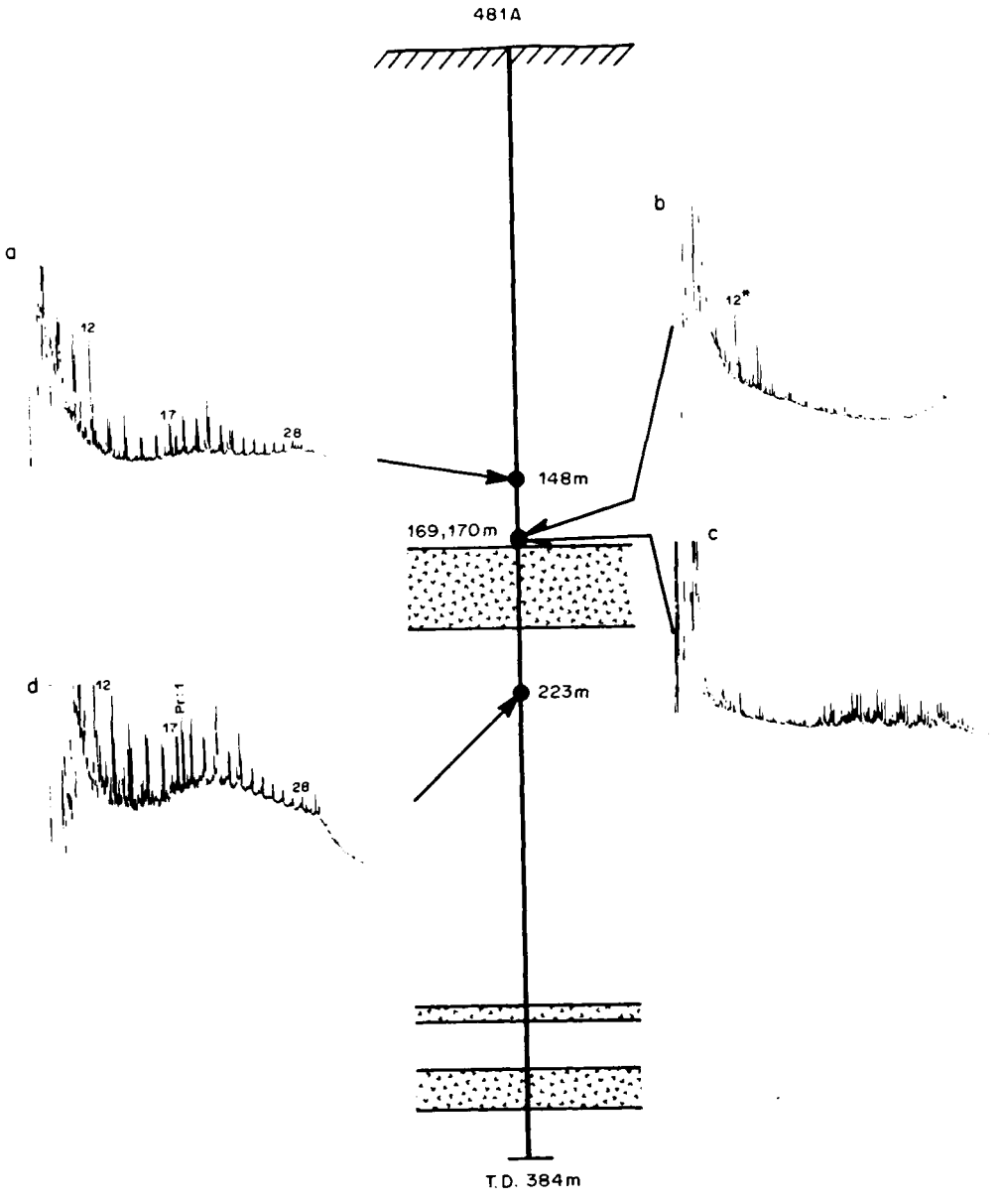

Fig. 19. Examples of Cupy–GC traces for kerogens from Site 481 shown versus sub-bottom depth: (a) 481A-12-1, 107-109 cm; (b) 481A-14-3, 50–52 cm; (c) 481A-14-4, 2–4 cm; (d) 481A-20-1, 60–62 cm.

ated by alkene/alkane doublets ranging from C_{10} to C_{30} and maximizing between C_{18} and C_{20}. The presence both of prist-1-ene and prist-2-ene in a ratio of about 1 : 1 and the steranes and triterpanes suggests that the sample has undergone only limited alteration. Previous pyrograms in this study indicate that prist-2-ene, as well as steranes and triterpanes are absent if the sample has been substantially altered.

Sample 481A-14-3, 50–52 cm is one of three from the immediate vicinity of the sill complex. The pyrogram (Fig. 19b) has many characteristics of previous samples that were extensively altered. The amount of pyrolyzable material is low and its source is unknown. The multiplet in the n-C_{12} region is the dominant feature and the pyrogram generally lacks other interpretable information.

Sample 481A-14-4, 2–4 occurs only one meter deeper than 481A-14-3, 50–52 cm, and its kerogen pyrogram (Fig. 19c) lacks any evidence of alkene/alkane doublets. Instead, seven or eight broad humps in the C_{17}–C_{30} region are the major features. On each hump is a triplet of peaks, which appear to form three homologous series. This pyrogram has only a small multiplet in the n-C_{12} region.

Sample 481A-14-4, 52–54 cm is 50 cm lower than 481A-14-4, 2–4 cm, and its kerogen pyrogram is very similar. The series of broad humps and associated

triplets are present. This sample has a significant multiplet in the C_{12} region, plus a complex distribution of other components in the lower-molecular-weight region.

These pyrograms are quite different from any others for thermally-altered kerogens in this study. The multiple emplacement of the sill complex (Simoneit, 1982d; Einsele *et al.*, 1980) in this hole indicates that these two samples may represent "bituminized kerogens" (Peters *et al.*, 1979). The "pressure-cooking" effect on the trapped kerogen and liquids produced by thermal degradation of the organic material could cause them to recombine and form a coke-like material similar to mesophase formation in coal (Durand, 1980b; Van Krevelen, 1961).

Sample 481A-18-1, 27–29 cm occurs immediately below the sill and the pyrogram of this kerogen gives no indication of any extensive alteration. The extract shows no fluorescence, which also indicates no major thermal alteration (Simoneit, 1982d). The dominant features of the pyrogram are the alkene/alkane doublets ranging from C_9 to C_{31}, with no odd/even carbon-number-predominance, and maximizing at C_{20}. Prist-1-ene and prist-2-ene also occur in approximately equal amounts. The pyrogram is very similar in appearance to that of sample 481A-20-1, 60–62 cm in Fig. 19d.

The kerogen pyrogram of sample 481A-20-1, 60–62 cm (Fig. 19d) is nearly identical to the shallow samples and Walvis Bay diatomaceous ooze pyrograms (Simoneit and Philp, 1982). Alkene/alkane doublets occur throughout the pyrogram and are predominant below C_{20}. Prist-1-ene and prist-2-ene are present in a 1 : 1 ratio and are more abundant than the C_{17} doublet. Steranes and triterpanes in the C_{30} region and complex unresolved humps are prominent features of the pyrogram.

Therefore, it appears that the two samples below the sill are essentially unaffected by the thermal effects of the intrusion, and little alteration has occurred from burial maturation or by diagenesis.

SUMMARY AND CONCLUSIONS

Lipids and kerogens were analyzed from samples at various depths and near intrusive sills at Sites 474, 477-479, and 481. The lipids were characterized by their homolog distributions, molecular markers, and unresolvable components to assess their genetic sources (cf. Simoneit *et al.*, 1984) and the thermal alteration caused by the intrusions. The kerogens were analyzed for their pyrolysis products (a measure of thermal maturity) and for the sources of the carbon in the kerogen (Simoneit *et al.*, 1984).

Site 474

The lipids from the shallow samples at the mouth of the Gulf of California are of an autochthonous marine origin and were deposited under oxic conditions (Simoneit, 1982c). The kerogen from Site 474 is unaltered and similar to shallow samples from the other sites.

Site 477

Lipids from the shallow samples at Site 477 are primarily of an autochthonous marine origin, with minor terrestrial plant waxes. Sedimentation was partially euxinic, probably due to the high deposition rates of organic detritus. Near and below the sill, the lipids are thermally altered. This is indicated on approaching the sill by a loss of the odd/even carbon-number-predominance of the *n*-alkanes, the appearance of a broad, unresolved hump, and the isomerization and generation of mature molecular markers. Large amounts of olefins (occurring only in the altered samples from Sites 477 and 481) and elemental sulfur are also present. Thermal alteration of lipids is most severe at Site 477.

Unaltered kerogens from samples 477-5-1, 81–91, 94–96 cm and 477-5-cc are nearly identical to surface samples from all the other sites. Sample 477-7-1, 124–126 cm a few meters above the sill, shows signs of being altered, presumably as a result of the intrusion. Nearer the sill, sample 477-7-2, 14–16 cm shows even more dramatic alteration. A characteristic of these thermally-altered samples is a multiplet of peaks in the *n*-C_{12} region of the pyrogram. Kerogens from sections 477-17-3 and 477-20-2 give pyrograms similar in appearance to that of Section 477-7-2, indicating a high degree of thermal alteration. Section 477-22-1, 75 m below the bottom of the sill, produces a pyrogram showing some signs of alteration, as indicated by the multiplet in the *n*-C_{12} region. It also has some characteristics of the unaltered samples. This sample probably has not been affected as much by the sill as by the high heat flow from depth (Curray *et al.*, 1982; Einsele *et al.*, 1980). Finally, the two deepest samples, from Sections 477A-5-1 and 477A-9-1, yield similar pyrograms and appear to be more altered than the samples from Section 477-22-1. High heat flow from greater depth has probably played a more important role in the alteration of these samples than the sill intrusion.

Site 478

In the shallow samples, the lipids are derived from marine and allochthonous terrigenous sources in about equal proportions (cf. Simoneit *et al.*, 1984). They were deposited under partially euxinic conditions, again due to the high sedimentation rates of organic detritus. The lipids in samples from greater depths are essentially unaltered (e.g. in Section 478-35-2) unless they are near sills. The deep, unaltered samples reflect the same sources and depositional conditions as the shallow samples. The distributions of the homologous compounds, the hump, and the degree of isomerization of molecular markers (e.g. triterpanes) indicate that the lipids of the altered samples have experienced lower thermal stress than those from Site 477.

For the kerogens, thermal alteration increases with depth, as is observed for Site 477. The effect of alteration is first noticeable (in the pyrogram) in sample 478-29-2, 108–110 cm, near the sill (about 255 m). Unlike Site 477 there is no obvious evidence for a "pressure-cooker" effect on the organic matter trapped between the sill intrusions. The sills are responsible for most of the thermal alteration in these samples.

Site 481

The lipids from shallow samples in the northern rift are primarily from terrigenous sources, with a minor component of autochthonous marine detritus (cf. Simoneit *et al.*, 1984). On the continental slope at Site 479, however, these two sources are about equivalent. The environmental conditions were partially euxinic (as in the other areas) because of the high sedimentation rates of organic detritus. The lipids of the thermally-altered samples indicate a similar stress as at Site 478. The carbon-number-predominance of the *n*-alkanes is lost, a broad hump is present, and molecular markers have undergone isomerization. Compared to Site 478, lesser amounts of sulfur are present, and olefins occur only in sample 481A-14-4, 52–54 cm, near the sill complex.

The kerogens from three samples above the sill complex show signs of thermal alteration. Two samples (481A-14-4, 2–4 cm, and 481A-14-4, 52–54 cm) are unique. A series of phenolic-type humps in their pyrograms suggest a recombination of kerogen and liquid products in a "pressure-cooker" environment. Below the sill complex, the samples were not affected by the sill and the pyrograms are similar to those of shallow samples or Walvis Bay diatomaceous ooze.

Thermal alteration of protokerogen at Sites 477, 478 and 481 occurred due to the intrusions of dolerite sills. Kerogen atomic H/C values as low as 0.4 occur near the sills. During alteration, ESR line width passes through a maximum of 6.5 gauss at an H/C of about 0.64. ESR *g*-value, on the other hand, shows no correlation with maturity, perhaps due to the presence of humic acids in the samples.

Atomic N/C, carbon isotope composition, and ESR spin density all show the effects of thermal stress near the sills. Their behavior, however, is not uniform among the three sites. At Sites 477 and 481, N/C values decrease near the sills to 0.025 and less. In contrast, N/C values near the small sill at Site 478 remain as high as 0.05. The $\delta^{13}C$ values decrease by 1–1.5‰ near the sills at Sites 477 and 481, whereas they increase slightly at Site 478. Finally, spin density reaches higher values at Site 477 than at Site 478, and the maximum occurs at a lower H/C ratio. These incongruities do not seem to be a result of compositional differences but may reflect differences in sill thickness (and hence intensity and duration of thermal stress) at the three sites. It is proposed that a thermally labile, isotopically heavy, and nitrogen-rich component of the Guaymas Basin protokerogen was altered more at Sites 477 and 481 than at Site 478. The chemical and isotopic heterogeneity of recently-deposited protokerogen may thus cause a more complex response to thermal stress than that expected for a diagenetically-mature kerogen.

Acknowledgements—We thank Ms Dara Blumfield and Ms Dana Blumfield for technical assistance, Mr E. Ruth for GC–MS data acquisition, Mr D. Winter for stable isotope determinations, Drs L. A. Kodina, M. P. Bogacheva and V. G. Shirinsky for data and assistance, and Drs K. E. Peters and J. E. Zumberge for reviews and suggestions for improvement of this manuscript. Partial financial support from the U.S. National Science Foundation, Division of Ocean Sciences (Grants OCE81-18897 and OCE83-12036) is gratefully acknowledged.

REFERENCES

Abelson P. H. and Hoering T. C. (1961) Carbon isotope fractionation in formation of amino acids by photosynthetic organisms. *Proc. Nat. Acad. Sci.* **47**, 623–632.

Ageta H., Shioima K. and Arai Y. (1968) Fern constituents: Neohopane, hopene-II, neohopadiene and fernadiene isolated from *Adiantum* species. *Chem. Commun.* **1968**, 1105–1107.

Austen D. E. G., Ingram D. J. E., Given P. H., Binder C. R. and Hill L. W. (1966) Electron spin resonance study of pure macerals. In *Coal Science* (Edited by Given P. H.), pp. 344–362. *Adv. Chem. Ser.* No. 55, Am. Chem. Soc., Washington, DC.

Baker E. W. and Louda J. W. (1982) Geochemistry of tetrapyrrole, tetraterpenoid and perylene pigments in sediments from the Gulf of California: Deep Sea Drilling Project Leg 64, Sites 474, 477, 479 and 481, and Scripps Institution of Oceanography Guaymas Basin survey cruise Leg 3, sites 10G and 18G. In *Initial Reports of the Deep Sea Drilling Project* (Edited by Curray J. R. *et al.*), Vol. 64, pp. 789–814. U.S. Govt Printing Office, Washington, DC.

Baker E. W. and Louda J. W. (1983) Thermal aspects of chlorophyll geochemistry. In *Advances in Organic Geochemistry 1981* (Edited by Bjorøy M. *et al.*), pp. 401–421. Wiley, Chichester.

Baker E. W., Huang W. Y., Rankin J. G., Castano J. R., Guinn J. R. and Fuex A. N. (1978) Electron paramagnetic resonance study of thermal alteration of kerogen in deep-sea sediments by basaltic sill intrusion. In *Initial Reports of the Deep Sea Drilling Project* (Edited by Lancelot Y. *et al.*), Vol. 41, pp. 839–847. U.S. Govt Printing Office, Washington, DC.

Bracewell J. M., Robertson G. W. and Tate K. R. (1976) Pyrolysis gas chromatography studies on a climosequence of soils in Tussock Grasslands, New Zealand. *Geoderma* **15**, 109–215.

Calvert S. E. (1964) Factors affecting distributions of laminated diatomaceous sediments in Gulf of California. In *Marine Geology of the Gulf of California* (Edited by van Andel T. H. and Shor G. G.), pp. 311–330. Am. Assoc. Petrol. Geol. Mem. 3, Tulsa.

Calvert S. E. (1966) Origin of diatom-rich, varved sediments from the Gulf of California. *J. Geol.* **76**, 546–565.

Chesnut D. B. (1977) On the use of the AW^2 method for integrated line intensities from first derivative presentations. *J. Mag. Res.* **25**, 373–374.

Cooper J. E. and Bray E. E. (1963) A postulated role of fatty acids in petroleum formation. *Geochim. Cosmochim. Acta* **29**, 1113–1127.

Curray J. R., Moore D. G., Aguayo J. E., Aubry M. P., Einsele G., Fornari D. J., Gieskes J., Guerrero J. C., Kastner M., Kelts K., Lyle M., Matoba Y., Mollina-Cruz A., Niemitz J., Rueda J., Saunders A. D., Schrader H., Simoneit B. R. T. and Vacquier V. (1979) Leg 64 seeks

evidence on development of basin in the Gulf of California. *Geotimes* **24**(7), 18–20.

Curray J. R., Moore D. G., Aguayo J. E., Aubry M. P., Einsele G., Fornari D. J., Gieskes J., Guerrero J. C., Kastner M., Kelts K., Lyle M., Matoba Y., Mollina-Cruz A., Niemitz J., Rueda J., Saunders A. D., Schrader H., Simoneit B. R. T. and Vacquier V. (1982) *Initial Reports of the Deep Sea Drilling Project*, Vol. 64, Parts I and II, 1313 pp. U.S. Government Printing Office, Washington, DC.

Davis J. B. and Stanley J. P. (1982) Catalytic effect of smectite clays in hydrocarbon generation revealed by pyrolysis–gas chromatography. *J. Anal. Appl. Pyrol.* **4**, 227–240.

DeJongh D. C. (1977) Pyrolytic reaction mechanisms. In *Analytical Pyrolysis, Proc. 3rd Int. Symp. on Anal. Pyrol.* Amsterdam 1976 (Edited by Jones C. E. R. and Cramers C. A.), pp. 261–275. Elsevier, Amsterdam.

Didyk B. M., Simoneit B. R. T., Brassell S. C. and Eglinton G. (1978) Geochemical indicators of paleoenvironmental conditions of sedimentation. *Nature* **272**, 216–222.

Durand B. (1980a) Sedimentary organic matter and kerogen, definition and quantitative importance of kerogen. In *Kerogen* (Edited by Durand B.), pp. 13–34. Editions Technip, Paris.

Durand B. (Ed.) (1980b) *Kerogen, Insoluble Organic Matter from Sedimentary Rocks*, 519 pp. Editions Technip, Paris.

Durand B. and Monin J. C. (1980) Elemental analysis of kerogens (C, H, O, N, S, Fe). In *Kerogen* (Edited by Durand B.), pp. 113–142. Editions Technip, Paris.

Durand B., Marchand A., Amiell J. and Combaz A. (1977) Étude de kérogènes par résonance paramagnétique electronique. In *Advances in Organic Geochemistry 1975* (Edited by Campos R. and Goñi J.), pp. 753–779. ENADIMSA, Madrid.

Einsele G., Gieskes J. M., Curray J., Moore D. G., Aguayo E., Aubry M. P., Fornari D., Guerrero J., Kastner M., Kelts K., Lyle M., Matoba Y., Mollina-Cruz A., Niemitz J., Rueda J., Saunders A., Schrader H., Simoneit B. R. T. and Vacquier V. (1980) Intrusion of basaltic sills into highly porous sediments, and resulting hydrothermal activity. *Nature* **283**, 441–445.

Frazer J. W. (1962) Simultaneous determination of carbon, hydrogen and nitrogen. Part II. *Mikrochim. Acta* **6**, 993–999.

Galimov E. M. (1974) Organic geochemistry of carbon isotopes. In *Advances in Organic Geochemistry 1973* (Edited by Tissot B. and Bienner F.), pp. 439–452. Editions Technip, Paris.

Galimov E. M. (1980) Organic geochemistry of carbon isotopes. In *Kerogen* (Edited by Durand V.), pp. 439–452. Editions Technip, Paris.

Galimov E. M. and Kodina L. A. (1983) Organic matter in oceanic sediments of high thermogradient (DSDP Leg 64, Gulf of California). In *Advances in Organic Geochemistry 1981* (Edited by Bjorøy M. *et al.*), pp. 431–437. Wiley, Chichester.

Galimov E. M., Kodina L. A., Bogacheva M. P. and Shirinsky V. G. (1982) Organic geochemical studies of samples from Deep Sea Drilling Project Leg 64, Gulf of California: Sites 474, 477, 478, 479 and 481. In *Initial Reports of the Deep Sea Drilling Project* (Edited by Curray J. R. *et al.*), Vol. 64, pp. 819–836. U.S. Govt Printing Office, Washington, DC.

Gallegos E. J. (1975) Terpane–sterane release from kerogen by pyrolysis GC–MS. *Anal. Chem.* **47**, 1524–1528.

Gilbert D. and Summerhayes C. P. (1982) Organic facies and hydrocarbon potential in the Gulf of California. In *Initial Reports of the Deep Sea Drilling Project* (Edited by Curray J. R. *et al.*), Vol. 64, pp. 864–870. U.S. Govt Printing Office, Washington, DC.

Ho T. T. Y. (1979) Geological and geochemical factors controlling electron spin resonance signals in kerogen. *UNESCAP/CCOP Tech. Publ.*, No. 6, pp. 54–80.

Hoefs J. and Frey M. (1976) The isotopic composition of carbonaceous matter in a metamorphic profile from the Swiss Alps. *Geochim. Cosmochim. Acta* **40**, 945–951.

Howard D. L. (1980) Polycyclic triterpenes of the anaerobic photosynthetic bacterium, *Rhodomicrobium vannielii*. Ph.D. Thesis, University of California, Los Angeles, 272 pp.

Howard D. L., Simoneit B. R. T. and Chapman D. J. (1984) Triterpenoids from lipids of *Rhodomicrobium vannielii*. *Arch. Microbiol.* **137**, 200–204.

Huang W.-Y. and Meinschein W. G. (1979) Sterols as ecological indicators. *Geochim. Cosmochim. Acta* **43**, 739–745.

Huc A. Y., Hunt J. M. and Whelan J. K. (1981) The organic matter of a Gulf Coast well studied by a thermal analysis–gas chromatography technique. *J. Geochem. Explor.* **15**, 671–681.

Irwin W. J. (1979a) Analytical pyrolysis—an overview. *J. Anal. Appl. Pyrol.* **1**, 3–25.

Irwin W. J. (1979b) Analytical pyrolysis—an overview. *J. Anal. Appl. Pyrol.* **1**, 89–122.

Ishiwatari R., Ishiwatari M., Rohrback B. G. and Kaplan I. R. (1977) Thermal alteration expriments on organic matter from recent marine sediments in relation to petroleum genesis. *Geochim. Cosmochim. Acta* **41**, 815–828.

Jenden P. D. (1983) Maturation of organic matter in the Paleocene–Eocene Wilcox group, South Texas, relationship to clay diagenesis and sandstone cementation. Ph.D. Thesis, University of California, Los Angeles, 274 pp.

Jenden P. D., Simoneit B. R. T. and Philp R. P. (1982) Hydrothermal effects on protokerogen of unconsolidated sediments from Guaymas Basin, Gulf of California; elemental compositions, stable carbon isotope ratios and electron-spin resonance spectra. In *Initial Reports of the Deep Sea Drilling Project* (Edited by Curray J. R. *et al.*), Vol. 64, pp. 905–912. U.S. Govt Printing Office, Washington, DC.

Jones C. E. R. and Cramers C. A. (Eds) (1977) *Analytical Pyrolysis, Proc. 3rd Int. Symp. on Anal. Pyrolysis.* Elsevier, Amsterdam.

Kendrick J. W. (1982) Petroleum-generating potential of sediment in the Gulf of California. In *Initial Reports of the Deep Sea Drilling Project* (Edited by Curray J. R. *et al.*), Vol. 64, pp. 865–870. U.S. Govt Printing Office, Washington, DC.

Larter S. R. (1984) Application of analytical pyrolysis techniques to kerogen characterization and fossil fuel exploration and exploitation. *Proc. 3rd Int. Conf. Anal. and Appl. Pyrol.* (in press).

Larter S. R. and Douglas A. G. (1978) Low molecular weight aromatic hydrocarbons in coal maceral pyrolysates as indicators of diagenesis and organic matter type. In *Environmental Biogeochemistry and Geomicrobiology* (Edited by Krumbein W. E.), Vol. 1, pp. 373–386. Ann Arbor Science Publishers, Ann Arbor.

Larter S. R., Solli H., Douglas A. G., de Lange F. and de Leeuw J. W. (1979) The occurrence and significance of prist-1-ene in kerogen pyrolysates. *Nature* **279**, 405–407.

Mackenzie A. S., Brassell S. C., Eglinton G. and Maxwell J. R. (1982a) Chemical fossils: The geological fate of steroids. *Science* **217**, 491–504.

Mackenzie A. S., Lamb N. A. and Maxwell J. R. (1982b) Steroid hydrocarbons and the thermal history of sediments. *Nature* **295**, 223–226.

Marchand A. and Conard J. (1980) Electron paramagnetic resonance in kerogen studies. In *Kerogen* (Edited by Durand B.), pp. 243–270. Editions Technip, Paris.

Maters W. L., van de Meent, D., Schuyl P. J. W., de Leeuw

J. W., Schenck P. A. and Meuzelaar H. L. C. (1977) Curie point pyrolysis in organic geochmistry. In *Analytical Pyrolysis, Proc. 3rd Int. Symp. on Anal. Pyrolysis* (Edited by Jones C. E. R. and Cramers C. A.), pp. 203–216. Elsevier, Amsterdam.

McKirdy D. M. and Powell T. G. (1974) Metamorphic alteration of carbon isotopic composition in ancient sedimentary organic matter: New evidence from Australia and South Africa. *Geology* **2**, 591–595.

Meuzelaar H. L. C., Haider K., Nagar B. R. and Martin A. J. P. (1977) Comparative studies on pyrolysis mass spectra of melanins, model phenolic polymers and humic acids. *Geoderma* **17**, 239–252.

Monson K. D. and Hayes J. M. (1982) Carbon isotopic fractionation in the biosynthesis of bacterial fatty acids. Ozonolysis of unsaturated fatty acids as a means of determining the intramolecular distribution of carbon isotopes. *Geochim. Cosmochim. Acta* **46**, 139–149.

Morishima H. and Matsubayashi H. (1978) ESR diagram: A method to distinguish vitrinite macerals. *Geochim. Cosmochim. Acta* **42**, 537–540.

Nissenbaum A. and Kaplan I. R. (1972) Chemical and isotopic evidence for the *in situ* origin of marine humic substances. *Limnol. Oceanogr.* **17**, 570–582.

Peters K. E. (1978) Effects on sapropelic and humic protokerogen during laboratory-simulated geothermal maturation experiments. Ph.D. Thesis, University of California, Los Angeles, 172 pp.

Peters K. E., Rohrback B. G. and Kaplan I. R. (1981) Carbon and hydrogen stable isotope variations in kerogen during laboratory-simulated thermal maturation. *Am. Assoc. Pet. Geol. Bull.* **65**, 501–508.

Peters K. E., Simoneit B. R. T., Brenner S. and Kaplan I. R. (1979) Vitrinite reflectance-temperature determinations for intruded Cretaceous black shale in the Eastern Atlantic. In *Symp. on Low Temperature Metamorphism: Kerogen and Clay Minerals* (Edited by Oltz D. F.), pp. 53–58. Pacific Section, SEPM, Los Angeles.

Peters K. E. and Simoneit B. R. T. (1982) Rock-Eval pyrolysis of Quaternary sediments from Leg 64, Sites 479 and 480, Gulf of California. In *Initial Reports of the Deep Sea Drilling Project* (Edited by Curray J. R. *et al.*), Vol. 64, pp. 925–931. U.S. Govt Printing Office, Washington, DC.

Philp R. P., Calvin M., Brown S. and Yang E. (1978) Organic geochemical studies on kerogen precursors in recently-deposited algal mats and oozes. *Chem. Geol.* **22**, 207–231.

Posthumus M. A., Nibbering N. M. M., Boerboom A. J. H. and Schulten H. R. (1974) Pyrolysis mass spectrometric studies on nucleic acids. *Biomed. Mass Spectrom.* **1**, 352–367.

Posthumus M. A. and Nibbering N. M. M. (1977) Pyrolysis mass spectrometry of methionine. *Org. Mass Spectrom.* **12**, 334–337.

Pusey W. C. (1973) Paleotemperatures in the Gulf Coast using the ESR-kerogen method. *Trans. Gulf Coast Assoc. Geol. Sci.* **23**, 195–212.

Rohrback B. G., Peters K. E., Sweeney R. E. and Kaplan I. R. (1983) Ammonia formation in laboratory simulated thermal maturation: Implications related to the origin of nitrogen in natural gas. In *Advances in Organic Geochemistry 1981* (Edited by Bjorøy M. *et al.*), pp. 819–823. Wiley, Chichester.

Schrader H., Kelts K., Curray J., Moore D., Aguayo E., Aubry M. P., Einsele G., Fornari D., Gieskes J., Guerrero J., Kastner M., Lyle M., Matoba Y., Mollina-Cruz A., Niemitz J., Rueda J., Saunders A., Simoneit B. R. T. and Vacquier V. (1980) Laminated diatomaceous sediments from the Guaymas Basin slope (Central Gulf of California): 250,000-year climate record. *Science* **207**, 1207–1209.

Schulten H. R., Beckey H. D., Meuzelaar H. L. C. and Boerboom A. J. H. (1973) High resolution field ionization mass spectrometry of bacterial pyrolysis products. *Anal. Chem.* **45**, 191–195.

Schulten H. R., Gortz W. and Stembridge C. H. (1978) Curie-point pyrolysis and field ionization mass spectrometry of polysaccharides. *Anal. Chem.* **50**, 428–433.

Seifert W. K. and Moldowan J. M. (1979) The effect of biodegradation on steranes and terpanes in crude oil. *Geochim. Cosmochim. Acta* **43**, 111–126.

Simmonds P. G., Schulman G. P. and Stembridge C. H. (1969) Organic analysis by pyrolysis gas chromatography–mass spectrometry. A candidate experiment for the biological exploration of Mars. *J. Chrom. Sci.* **7**, 36–41.

Simoneit B. R. T. (1975) Sources of organic matter in oceanic sediments. Ph.D. Thesis, University of Bristol, England, 300 pp.

Simoneit B. R. T. (1977a) Leg 41 sediment lipids—Search for eolian organic matter in Recent samples and examination of a black shale. In *Initial Reports of the Deep Sea Drilling Project* (Edited by Lancelot Y. *et al.*), pp. 855–858. U.S. Govt Printing Office, Washington, DC.

Simoneit B. R. T. (1977b) Diterpenoid compounds and other lipids in deep-sea sediments and their geochemical significance. *Geochim. Cosmochim. Acta* **41**, 463–476.

Simoneit B. R. T. (1978) The organic chemistry of marine sediments. In *Chemical Oceanography* (Edited by Riley J. P. and Chester R.), 2nd edn, Vol. 7, pp. 233–311. Academic Press, New York.

Simoneit B. R. T. (1981) Utility of molecular markers and stable isotope compositions in the evaluation of sources and diagenesis of organic matter in the geosphere. In *The Impact of the Treibs' Porphyrin Concept on the Modern Organic Geochemistry* (Edited by Prashnowsky A. A.), pp. 133–158. Bayerische Julius Maximilian Universität, Würzburg.

Simoneit B. R. T. (1982a) The composition, sources and transport of organic matter to marine sediments—the organic geochemical approach. In *Proc. Symp. Marine Chem. into the Eighties* (Edited by Thompson J. A. J. and Jamieson W. D.), pp. 82–112. Nat. Res. Council of Canada, Ottawa.

Simoneit B. R. T. (1982b) Some applications of computerized GC–MS to the determination of biogenic and anthropogenic organic matter in the environment. *Int. J. Environ. Anal. Chem.* **12**, 177–193.

Simoneit B. R. T. (1982c) Organic geochemistry of sediments from the mouth of the Gulf of California, Leg 64, Sites 474 and 476. In *Initial Reports of the Deep Sea Drilling Project* (Edited by Curray J. R. *et al.*), Vol. 64, pp. 877–880. U.S. Govt Printing Office, Washington, DC.

Simoneit B. R. T. (1982d) Shipboard organic geochemistry and safety monitoring, Leg 64, Gulf of California. In *Initial Reports of the Deep Sea Drilling Project* (Edited by Curray J. R. *et al.*), Vol. 64, pp. 723–728. U.S. Govt Printing Office, Washington, DC.

Simoneit B. R. T. (1983) Organic geochemistry of laminated sediments from the Gulf of California. In *Coastal Upwelling* (Edited by Suess E. and Thiede J.), Part A, pp. 527–543. Plenum, New York.

Simoneit B. R. T. (1984) Cyclic terpenoids of the geosphere. In *Biological Markers in the Sedimentary Record* (Edited by Johns R. B.). IGCP 157, Elsevier, Amsterdam (in press).

Simoneit B. R. T. and Mazurek M. A. (1981) Organic geochemistry of sediments from the Southern California Borderland, DSDP/IPOD Leg 63. In *Initial Reports of the Deep Sea Drilling Project* (Edited by Haq B. *et al.*), Vol. 63, pp. 837–853. U.S. Govt Printing Office, Washington, DC.

Simoneit B. R. T. and Philp R. P. (1982) Organic geochemistry of lipids and kerogen and the effects of basalt intrusions on unconsolidated oceanic sediments: Sites

477, 478 and 481, Guaymas Basin, Gulf of California. In *Initial Reports of the Deep Sea Drilling Project* (Edited by Curray J. R. *et al.*), pp. 883–904. U.S. Govt Printing Office, Washington, DC.

Simoneit B. R. T., Brenner S., Peters K. E. and Kaplan I. R. (1978) Thermal alteration of Cretaceous black shale by basaltic intrusions in the Eastern Atlantic. *Nature* **273**, 501–504.

Simoneit B. R. T., Mazurek M. A., Brenner S., Crisp P. T. and Kaplan I. R. (1979) Organic geochemistry of Recent sediments from Guaymas Basin, Gulf of California. *Deep-Sea Res.* **26A**, 879–891.

Simoneit B. R. T., Brenner S., Peters K. E. and Kaplan I. R. (1981) Thermal alteration of Cretaceous black shale by diabase intrusions in the Eastern Atlantic: II. Effects on bitumen and kerogen. *Geochim. Cosmochim. Acta* **45**, 1581–1602.

Simoneit B. R. T., Summerhayes C. P. and Meyers P. A. (1982) Sources, preservation and maturation of organic matter in Pliocene and Quaternary sediments of the Gulf of California: A synthesis or organic geochemical studies from Deep Sea Drilling Project Leg 64. In *Initial Reports of the Deep Sea Drilling Project* (Edited by Curray J. R. *et al.*), Vol. 64, pp. 939–952. U.S. Govt Printing Office, Washington, DC.

Simoneit B. R. T., Meyers P. A. and Summerhayes C. P. (1984) Organic matter in Quaternary sediments of the Gulf of California: A synthesis or organic geochemical studies from Deep Sea Drilling Project Leg 64. *Am. Assoc. Pet. Geol. Bull.* (in press).

Tissot B. P. and Welte D. H. (1978) *Petroleum Formation and Occurrence*, 538 pp. Springer, Berlin.

van de Meent D., Brown S. C., Philp R. P. and Simoneit B. R. T. (1980) Pyrolysis–high resolution gas chromatography and pyrolysis gas chromatography–mass spectrometry of kerogens and kerogen precursors. *Geochim. Cosmochim. Acta* **44**, 999–1013.

Van Krevelen D. W. (1961). *Coal*, 514 pp. Elsevier, Amsterdam.

Whelan J. K., Hunt J. M. and Huc A. Y. (1980) Applications of thermal distillation–pyrolysis to petroleum source rock studies and marine pollution. *J. Anal. Appl. Pyrol.* **2**, 79–96.

APPENDIX

Chemical Structures Cited

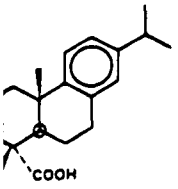

Dehydroabietic Acid

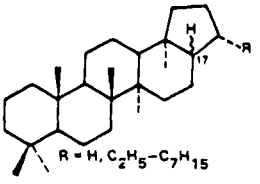

II. Hopanes

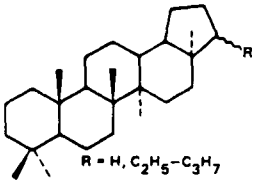

III. *iso*-Hopanes

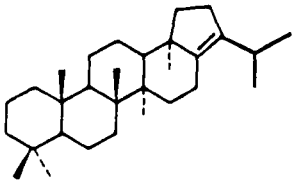

IV. Hop-17(21)-ene

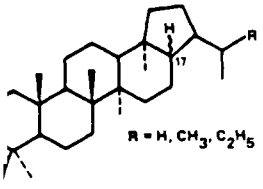

Moretanes

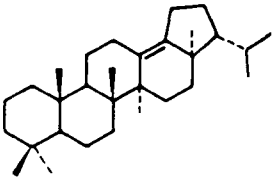

VI. *iso*-Hop-13(18)-ene

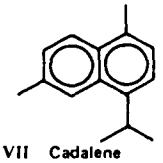

VII Cadalene

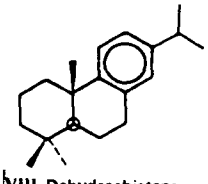

VIII. Dehydroabietane

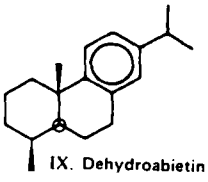

IX. Dehydroabietin

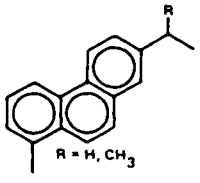

X. Retenes

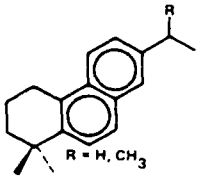

XI. Simonellites

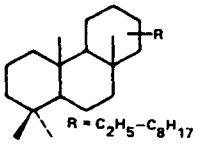

XII. Extended tricyclic terpanes

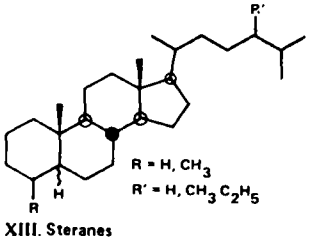

XIII. Steranes

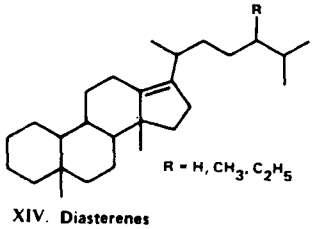

XIV. Diasterenes

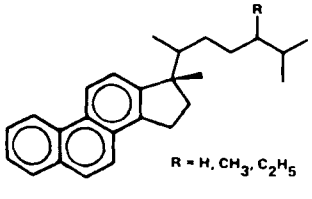

XV. Triaromatic Steranes

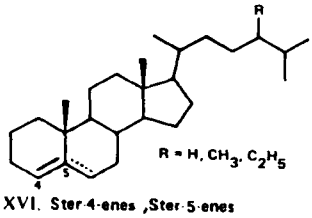

XVI. Ster-4-enes ,Ster-5-enes